Part One
Energy Production

1
Fossil Fuels: The Effect of Zeolite Catalyst Particle Morphology on Catalyst Performance in the Conversion of Methanol to Hydrocarbons

Katarzyna Anna Łukaszuk,[1,2] Pablo del Campo Huertas,[1] Andrea Molino,[1,2] Malte Nielsen,[1,2] Daniel Rojo-Gama,[1,2] Juan Salvador Martinez-Espin,[1,2] Karl Petter Lillerud,[1] Unni Olsbye,[1] Silvia Bordiga,[3] Pablo Beato,[2] and Stian Svelle[1]

[1]University of Oslo, Department of Chemistry, inGAP Center of Research Based Innovation, P.O. Box 1033, 0315 Oslo, Norway
[2]Haldor Topsøe A/S, Haldor TopsøesAllé 1, 2800 Kgs, Lyngby, Denmark
[3]NIS and INSTM Reference Centre, Department of Chemistry, Via Quarello 15, 10135 Torino, Italy

1.1
Zeolites and Zeotypes as Nanocatalysts for Petroleum and Natural Gas

A revolution occurred in the field of heterogeneous catalysis in the 1960s when zeolites were revealed to have a remarkable performance for acid-catalyzed processes [1,2]. The zeolites are used in fluid catalytic cracking, and thus are involved in the production of one-third of all gasoline. Other applications are hydrocracking, isomerization, selective catalytic reduction of nitrogen oxides, and the conversion of methanol to hydrocarbons. Zeolites are microporous, crystalline aluminosilicates, having pores and cavities with dimensions typically ranging from 3–12 Å, that is, in the nanometer or even subnanometer range. The building units of a zeolite are $[SiO_4]^{4-}$ and $[AlO_4]^{5-}$ tetrahedra, which can be linked together forming a huge number of different topologies. At present, 231 different structural types of zeolites exist [3].

A huge effort has been made into the synthesis of materials containing elements other than silicon and aluminum [4–6]. Examples of these zeolite-related (or zeotype) materials include aluminophosphates, gallophosphates (AlPOs, GaPOs), and silicoaluminophosphates (SAPOs) [4]. Metals such as Ti, Fe, V, Ge, Cr, and Mn have also been incorporated by isomorphic substitution into the framework, thereby providing unique acid and redox properties [7].

Zeolite synthesis requires sources of silicon, aluminum, and charge-balancing cations that are mixed in water at basic pH. In many cases, the presence of organic additives that act as structure-directing agents (or templates) is very important. These SDAs steer the crystallization toward the formation of a

Nanotechnology for Energy Sustainability, First Edition. Edited by Baldev Raj, Marcel Van de Voorde, and Yashwant Mahajan.

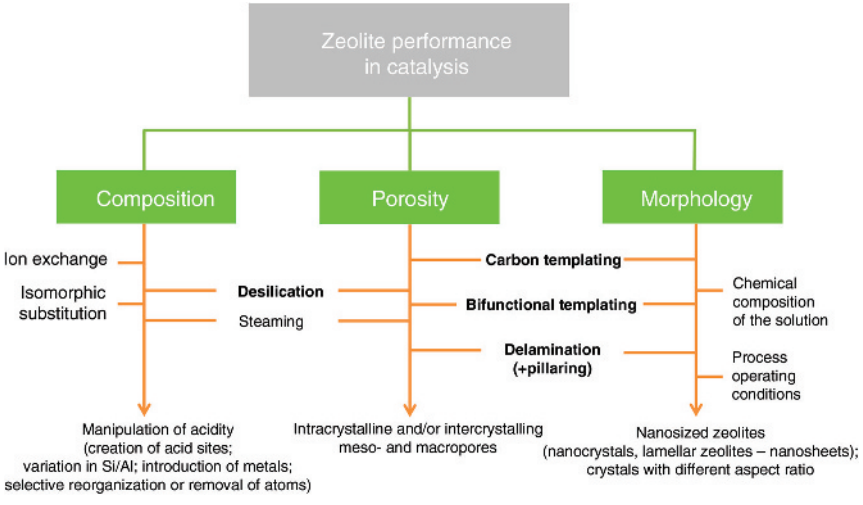

Figure 1.1 Various methods of affecting the catalytic performance of a zeolite. The approaches marked in bold are described in this chapter.

specific structure. Crystallization occurs in a sealed vessel in a temperature range 60–200 °C. Clearly, at such conditions it is hard to follow the ongoing chemical and physical processes related to crystallization, and much of the understanding is superficial and descriptive.

However, the zeolite nanostructure can be tailored not only during synthesis but also by postsynthetic treatments. Figure 1.1 provides an overview of the methods that can be applied. These widely investigated approaches are subdivided according to the parameter that is sought to be manipulated. Most of the preparation routes lead to changes in more than one parameter. As the topic of zeolite material design is very broad, in this chapter we describe only the methods that we believe hold the promise to perform rational materials design and show the resulting effects on the catalytic performance in the MTH reaction. For information about other synthetic approaches, we refer the reader to literature dedicated to zeolite synthesis [8–11]. In this contribution, we will highlight the effects of zeolite catalyst nanostructure, or morphology, on their performance in the industrially relevant conversion of methanol to hydrocarbons (MTH). Several variations of this process are currently being commercialized; with 20+ plants being constructed worldwide.

1.2 Modification of Porosity: Hierarchical Zeolites

Hierarchical zeolites consist of both micro- and mesopores/macropores in the same material. We can distinguish between bottom-up and top-down approaches to introduce such an additional pore system. The first method involves modification of the crystallization processes, whereas the second is a

postsynthetic treatment. Moreover, the routes differ in terms of versatility, effectiveness in porosity generation, applicability, and scalability [12].

1.2.1 Desilication in Alkaline Media

The alkaline-mediated desilication is a top-down postsynthetic treatment that allows creation of mesopores in premade zeolites. The desilication of zeolites was pioneered by Ogura *et al.* [13] and revitalized by Groen *et al.* [14]. Since then, the selective extraction of silicon from the zeolite framework through alkaline treatment has been widely investigated [14–20]. The alkaline solutions used in desilication of the ZSM-5 zeolite include, for example, NaOH, KOH, LiOH, and NH_4OH. Etching with HF is closely related. It was shown that sodium cations in the alkaline solution are required to achieve the highest efficiency [21]. Interestingly, the hydroxides of various organic ammonium cations commonly used to synthesize zeolites, such as tetrapropylammonium and tetrabutylammonium, can also lead to mesopore formation. In comparison to inorganic hydroxides, these organic bases are less reactive as concluded based on their slower desilication rate and less selective for Si extraction. However, organic compounds have an advantage over Na^+, that is, higher controllability of the desilication process. Other important parameters that affect desilication process include temperature, time of the treatment, base concentration, and also some features of a material submitted for modification. The influence of morphology and defects on the desilication of ZSM-5 has been demonstrated [20,22]. It was shown that for crystals with little intergrowths or defects, efficient desilication is limited to an optimal Si/Al ratio of 20 : 50. However, if the crystals possess many intergrowths and defects, the importance of the Si/Al ratio is reduced and the mesopores are mostly formed due to intergrowths/defect removal (Figure 1.2).

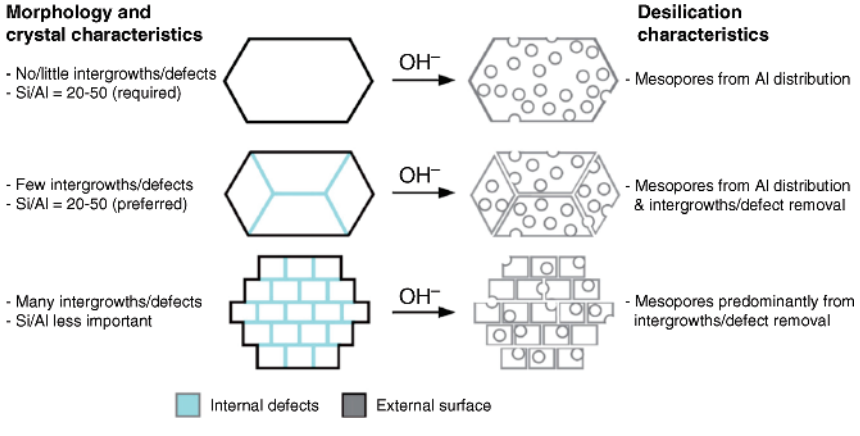

Figure 1.2 The relationships between effects of defects and intergrowths and framework Si/Al ratio on the mesopore formation during desilication. (Reprinted from Ref. [20] with permission from Elsevier.)

Table 1.1 Overview of framework types amenable to mesopore formation by desilication.

Framework	Si/Al ratio	Type of mesoporosity	References
MFI (3D)	12–200	Intracrystalline	[13,14,17,18,20,21,23–45]
FAU (3D)	28	Intracrystalline	[46]
CHA (3D)	14	Intracrystalline	[47]
BEA (3D)	35	Intracrystalline	[48–54]
FER(2D)	29	Intra- and intercrystalline	[14,55]
MWW(2D)	40	Not specified	[56]
MTW(1D)	58	Intracrystalline	[57]
MOR(1D)	20–30	Intracrystalline	[58–62]
TON(1D)	31–50	Intra- and intercrystalline	[63–67]
IFR(1D)	32	Intracrystalline	[68]
STF(1D)	29	Not specified	[69]
AST(0D)	31	Intercrystalline	[70]
TUN (3D)	20	Intracrystalline	[71]

Beato [22] confirmed that crystal defects have a significant influence on the desilication outcome. Thus, the alkaline treatment needs to be tailored for each specific batch of zeolite to obtain optimum results.

The alkaline-mediated desilication is an approach that is straightforward to use. Table 1.1 shows that it is also a versatile method that allows the introduction of an additional pore system to many different frameworks. However, it may have a profound impact on the acidity and crystallinity of zeolites. A clear understanding of the correlations between the changes of porous, textural, compositional, and acidic properties that occur upon desilication is necessary to utilize this postsynthetic method in the optimum manner for a given zeolite sample.

1.2.2 Carbon Templating

The carbon templating bottom-up method was originally developed for the synthesis of nanosized zeolites that crystallize within a porous carbon material, that is, confined space synthesis. The size of the final zeolite crystal is governed by pore size of carbon template. However, the formed zeolite crystals may contain a secondary mesopore system as a result of the packing and intergrowth of the small zeolite crystals, that is, intercrystalline pores. If the carbon material is incorporated within a single crystal, and once it is removed by calcination in air, an intracrystalline mesoporous zeolite is obtained [12]. The formation of both kinds of pore systems is illustrated in Figure 1.3.

Clearly, the size and shape of the intracrystalline mesopores will mirror that of the porous carbon (hard templating). Consequently, a broad range of carbonaceous

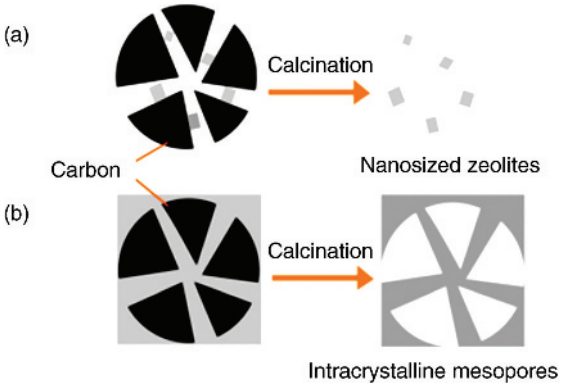

Figure 1.3 Illustrations of (a) the confined space synthesis method to obtain nanocrystals and (b) the formation of an additional mesoporosity in a single zeolite crystal.

materials exhibiting different shapes, sizes, and porosities, such as carbon particles, fibers, nanotubes, and colloidal imprinted carbon, have been explored [72]. In a very elegant work Jacobsen *et al.* [73] impregnated carbon black pearls with an excess of the synthesis gel to obtain ZSM-5-containing embedded carbon particles after crystallization. The carbon was burned off, leading to zeolite crystals with a secondary pore system. Schmidt *et al.* [74] synthesized MFI zeolite crystals with mesoporous system that exactly replicated the structure of the carbon nanotubes used.

There is still a lot to understand about the zeolite crystallization in the presence of carbon templates. Pérez-Pariente and Álvaro-Munoz [75] highlighted that the growth of the zeolite crystals around the carbonaceous materials should be related to the presence of an appropriate chemical interaction between the functional groups of the carbon template and the aluminosilicate species present in the synthesis medium. Little attention has been paid to the possible modification of this interaction in order to control synthesis, and consequently the properties of hierarchical materials. The authors notice that in most approaches, the zeolite is considered to be an "inert receptacle" for the "hard spheres" of carbon particles. A more thorough consideration of these chemical interactions could be very helpful in designing new materials with, for example, improved pore accessibility [75].

The carbon-templating approach can be applied to all zeolites and zeotypes. The method does in principle not affect the chemical composition or acidity of the material. The possibility of tailoring the size and connectivity of mesopores by varying the carbon employed is the great advantage of the method. However, the application of carbon templates has also some limitations, especially when production on the industrial scale is considered. Highly specialized carbons having the desired morphology, porosity, and purity can be expensive or need to be prepared in-house. Moreover, incorporation of the zeolite gel into the carbon can be challenging and may require complicated synthesis steps [12].

1.3
Modification of Size and Morphology

Crystal size is a function of the ratio between rate of nucleation and rate of growth [76]. As a consequence, synthesis of small zeolite crystals, which are often desired in catalysis (see below), takes place under conditions favoring nucleation over crystal growth [77]. The nucleation rate can be increased by optimization of parameters such as temperature, alkalinity (mineralizer), dilution, ionic strength, agitation, and aging. Furthermore, the protozeolitic species should be stabilized to prevent the formation of aggregates.

1.3.1
Nanozeolites

It is recognized that materials obtained from an aqueous phase have a tendency to agglomerate. In effect, large crystals (often undesired for catalytic reactions) are produced. However, an addition of organic medium can lead to the synthesis of nanocrystals. Vuong *et al.* reported a two-phase method (Figure 1.4) where nanosized silicate-1 (MFI) was received in the presence of both an organic (toluene) and an aqueous phase [78]. Hexadecyltrimethoxysilane was used as silylating agent to functionalize the zeolite seeds (prepared in water solution) with silane groups. The protozeolitic species thus become hydrophobic and enter and become dispersed in the organic solvent. The silanization prevents particle growth during subsequent hydrothermal crystallization of the two-phase mixture. Finally, two products with different size and morphology were synthesized: spherical and cubic nanocrystals (30–50 nm) in the toluene phase and micrometer sized (5 μm) coffin-like crystals in the aqueous phase.

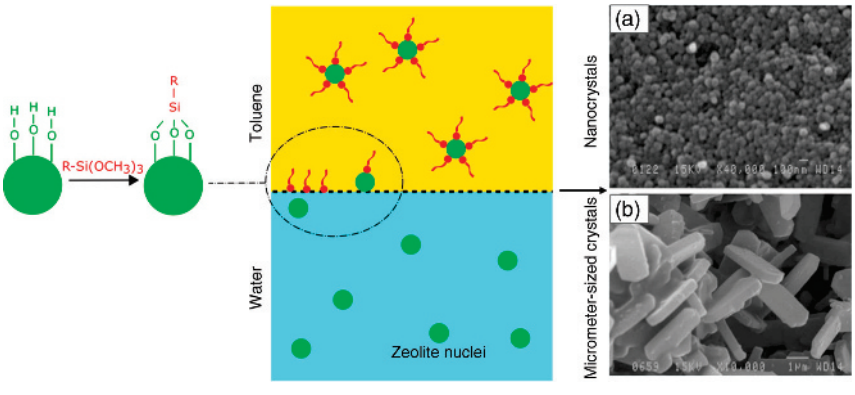

Figure 1.4 Schematic representation of the two-phase synthesis method. SEM image of silicalite-1 nanozeolites in the organic (toluene) phase (a) and micrometer-sized silicalite-1 crystals synthesized in the aqueous phase (b). (Adapted with permission from Ref. [78]. © Elsevier, 2009.)

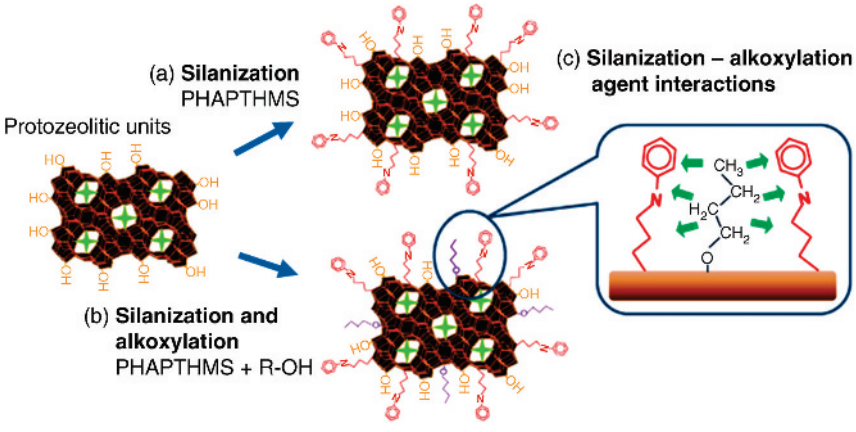

Figure 1.5 Diagram of ZSM-5 nanocrystal formation showing (a) the PHAPTMS surface silanization, (b) the incorporation of alkoxy moieties by alkoxylation when the silanization proceeds, and (c) the interaction between PHAPTMS and *n*-butoxy grafted species. (Reprinted from Ref. [82] with permission from Elsevier.)

To obtain exclusively a nanosized product, the authors proposed single-phase method [78]. In this approach, *n*-butanol was added to toluene, thereby increasing the miscibility of the organic and aqueous phases. As *n*-butanol is miscible with hydrocarbon solvent and moderately soluble in water, the resulting organic phase with lowered hydrophobicity disperses into the entire aqueous phase forming a "single phase" (in reality a dispersion). The hydrothermal synthesis of silicalite-1 (MFI) and faujasite (FAU) using a mixture of toluene with butanol provides nanocrystals of 20 and 25 nm, respectively [79].

Nanocrystals of MFI, BEA, FAU, and MOR can be also synthesized in an aqueous medium, when phenylaminopropyltrimethoxysilane (PHAPTMS) is applied for silanization of the zeolitic seeds obtained in a precrystallization step [80,81]. Serrano *et al.* [81] showed that synthesis of ZSM-5 is not successful if the precrystallization treatment is omitted. In such a case, the silanization species serves only as an additional silica source, obstructing completely the crystallization process. MFI prepared from silanized seeds tend to form aggregates that are comprised of nanocrystals with size <10 nm. Moreover, addition of alcohols in the silanization step was reported to improve the textural properties of the MFI zeolite, and this was explained by two effects, summarized in Figure 1.5 [82] – first, an increase in the degree of incorporation of PHAPTMS into the zeolite seeds; second, a stabilization of the hydrophobic organosilane layer.

1.3.2
Lamellar Zeolites

Lamellar zeolites can be seen as extended platelets with only one of the three dimensions limited to the nanometer size. Such 2D zeolites are attractive for

catalysis because of a high number of accessible catalytic sites on the external surface and reduced diffusion limitations that increase activity and reduce (the detrimental effects of) coke deposition.

The intensive work on lamellar zeolites started with a preparation of the a layered precursor MCM-22(P) [83], which can be seen as stacked zeolite layers containing the zeolite template occluded in the interlayer space. In contrast to the typical 3D zeolite frameworks, the layered precursor was demonstrated to be more flexible for structural modification. This is because the interlayer interaction is relatively weak. Subjecting those materials to appropriate postsynthetic treatments can therefore lead to separated sheets with nanometer thickness. Clearly, preparation of such lamellar materials is experimentally very challenging. Figure 1.6 shows the materials that can be prepared from the MCM-22(P) precursor phase. Upon calcination, the layers of MCM-22(P) connect and form the three-dimensional zeolite MCM-22 with a 10MR pore system. The related MCM-36 material is prepared by swelling MCM-22(P) in concentrated surfactant solutions and subsequent pillaring with a silica precursor [84]. Delamination of the swollen MCM-22 provides the ITQ-2 material with thickness of 2.5 nm.

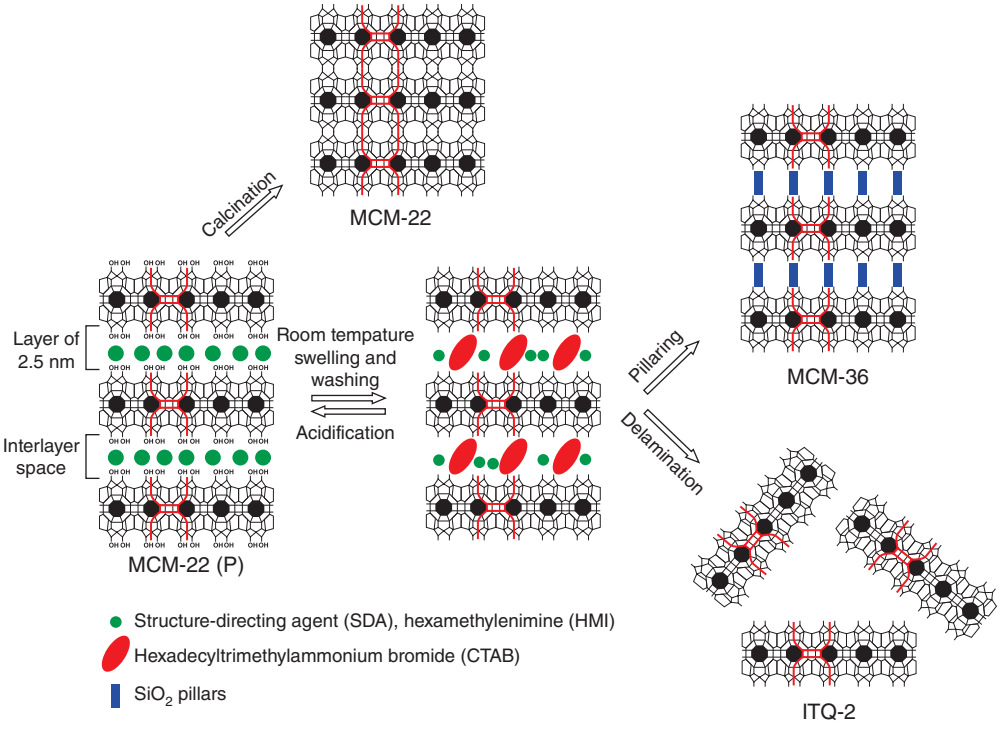

Figure 1.6 Various materials prepared from the layered precursor MCM-22(P). (Reprinted from Ref. [86] with permission from John Wiley & Sons, Inc.)

ABW	ACO	AEI	AEL	AEN	AET	AFG	AFI	AFN	AFO
AFR	AFS	AFT	AFV	AFX	AFY	AHT	ANA	APC	APD
AST	ASV	ATN	ATO	ATS	ATT	ATV	AVL	AWO	AWW
BCT	BEA	BEC	BIK	BOF	BOG	BOZ	BPH	BRE	BSV
CAN	CAS	CDO	CFI	CGF	CGS	CHA	CHI	CLO	CON
CSV	CZP	DAC	DDR	DFO	DFT	DOH	DON	EAB	EDI
EEI	EMT	EON	EPI	ERI	ESV	ETR	EUO	EWT	EZT
FAR	FAU	FER	FRA	GIS	GIU	GME	GON	GOO	HEU
IFO	IFR	IFW	IFY	IHW	IMF	IRN	IRR	IRY	ISV
ITE	ITG	ITH	ITN	ITR	ITT	ITV	ITW	IWR	IWS
IWV	IWW	JBW	JNT	JOZ	JRY	JSN	JSR	JST	JSW
KFI	LAU	LEV	LIO	LIT	LOS	LOV	LTA	LTF	LTJ
LTL	LTN	MAR	MAZ	MEI	MEL	MEP	MER	MFI	MFS
MON	MOR	MOZ	MRE	MSE	MSO	MTF	MTN	MTT	MTW
MVY	MWW	NAB	NAT	NES	NON	NPO	NPT	NSI	OBW
OFF	OKO	OSI	OSO	OWE	PAR	PAU	PCR	PHI	PON
POS	PSI	PUN	RHO	RON	RRO	RSN	RTE	RTH	RUT
RWR	RWY	SAF	SAO	SAS	SAT	SAV	SBE	SBN	SBS
SBT	SEW	SFE	SFF	SFG	SFH	SFN	SFO	SFS	SFV
SFW	SGT	SIV	SOD	SOF	SOS	SSF	SSO	SSY	STF
STI	STO	STT	STW	SVR	SVV	SZR	TER	THO	TOL
TON	TSC	TUN	UEI	UFI	UOS	UOV	UOZ	USI	UTL
UWY	VET	VFI	VNI	VSV	WEI	WEN	YUG	ZON	

Figure 1.7 Zeolite frameworks approved by the IZA Structure Commission – structures that have the layered forms are highlighted in orange [87,88].

This material has very high surface area and direct access to surface pockets that correspond to half a MCM-22 cage (indicated in red in Figure 1.6) [85,86].

The layered forms of other frameworks (Figure 1.7) have also been prepared, and for more details we refer the reader to recent excellent reviews [87,88].

Despite the success in preparation of lamellar zeolites, this has usually been a result of serendipity, rather than by a careful design strategy. This is a crucial difference when compared with the elegant approach described by Ryoo and coworkers. They have pioneered the application of bifunctional surfactants to produce single unit cell thick nanosheets of zeolite MFI [89]. The method relies on designing a diquaternary ammonium-type surfactant, $C_{22}H_{45}—N^+—(CH_3)_2—C_6H_{12}—N^+(CH_3)_2—C_6H_{13}$, that consists a structure-directing part and an alkyl chain that provides a hydrophobic environment for mesopore formation between the thin zeolite sheets. The assembly of the nanosheets occurs either as multilamellar stacks or in disordered unilamellar arrangements (Figure 1.8). Developing this idea further, Na *et al.* [90] synthesized surfactants with two symmetrical long alkyl tails linked by differently bridged ammonium groups. Using this type of SDAs, the resulting nanosheets of MFI zeolite were shaped into cylinders, creating an ordered mesoporous system [91].

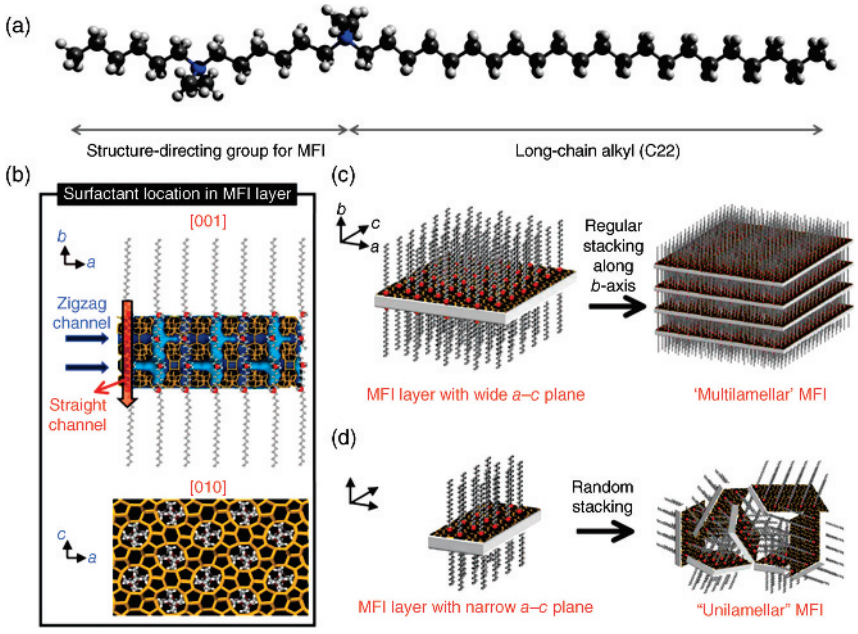

Figure 1.8 (a) Diquaternary ammonium-type surfactant. (b) Proposed structure model for the single MFI nanosheet. (c) Multilamellar stacking of MFI nanosheets along the *b*-axis. (d) A random assembly of MFI unilamellar structure. (Reprinted from Ref. [89] with permission from Nature Publishing Group.)

1.3.3
Zeolite Growth Modifiers

The introduction of foreign substances, often called growth modifiers, cosolvents (if liquid), or additives, is one of the methods to tailor size and morphology of organic and inorganic crystals. The compounds that have been investigated as modifiers range from ions and small molecules to macromolecules such as proteins and polymers [92]. An inspiration to develop this strategy was taken from an observation that small quantities of impurities can interact with higher energy crystal faces in such a way that their energy and growth rate is decreased. Consequently, the area of a facet that could even be absent for the crystal shape obtained without a growth modifier can be increased. In effect, the crystal growth is modified in an anisotropic way (Figure 1.9).

Leiserowitz and coworkers [94] showed that the chemical and structural heterogeneity of the crystal surfaces is key in a proper design or selection of a growth modifier. An additive has to possess an affinity to a particular surface in order to shape the crystal in the desired way. The influence of additives has been explored in the field of zeolites. The effects of, for example, alcohols and amines on the morphology of different frameworks have been explored (Table 1.2). As

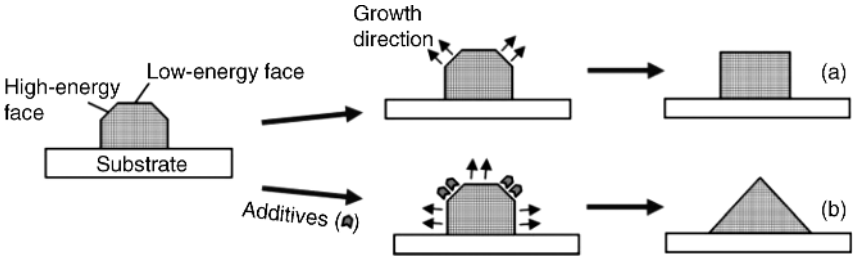

Figure 1.9 Crystal growth modification. a: According to the classic crystal growth theory, the surface of the slowest growing face (the low-energy face) is the one that dominates the final crystal morphology. b: Crystal shape can be modified by preferential adsorption of additives or growth modifiers. (Reprinted from Ref. [93] with permission from Royal Society of Chemistry.)

Table 1.2 Examples of growth modifiers that have been used in the synthesis of different zeolite frameworks.

Additives	Framework
Alcohols	TON [98], LTL [96,97,99], MOR [95,100], AFI [101], MTW [102], MFI [103], LTA [104]
Amines	LTL [97], LTA [105], AFI [101,106], MFI [107,108]
Organic acids	AFI [101,106], MFI [107]
Inorganic acids	AFI [101]
Inorganic salts	AFI [101], MFI [107], MOR [109]

zeolite crystallization is a very complex process, the mechanism of additive action is still not clear. Some studies support a hypothesis that the introduction of aliphatic alcohol causes a slower release of silicon and aluminum species from the aliphatic alcohol phase into the aqueous reaction medium. This leads to a reduced nucleation and consequently to the synthesis of larger crystals [95]. However, it was also shown that the addition of alcohols may decrease the aspect ratio of zeolite crystals [92,96,97]. For example, the introduction of 1,2,3-hexanetriol to the synthesis gel of zeolite LTL reduced the crystal growth along the c-direction, providing thin (<100 nm) crystals with disc-like shape (Figure 1.10a).

Lupulescu *et al.* postulate a mechanism involving the interaction of alcohols through hydrogen bonding with terminal hydroxyl groups of silicon and aluminum species on selected crystal surfaces [97]. Some alcohols and their isomers induce larger changes in crystal aspect ratio than others. As all the zeolite surfaces may possess OH groups, the results indicate that spatial arrangement of the additives and their functional groups can be a key feature of surface/additive matching that might allow tuning of the crystal morphology. Long, cylindrical LTL crystals were synthesized when PDDAC (polydiallyldimethylammonium chloride) was used as growth modifier (Figure 1.10b). In this case, electrostatic

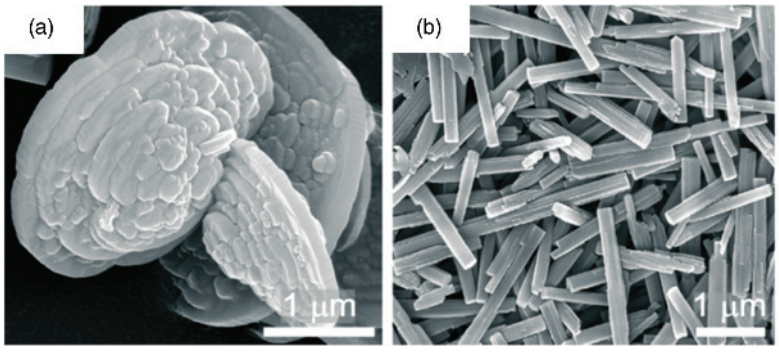

Figure 1.10 SEM images of (a) low-aspect-ratio disk-shaped crystals synthesized with addition of 1,2,3-hexanetriol, and (b) high-aspect-ratio rod-like crystals obtained using PDDAC. (Reprinted from Ref. [92] with permission from Royal Society of Chemistry.)

interactions were suggested to contribute to the adsorption of positively charged quaternary amines to the negatively charged 001 surface [92,97]. A limitation of the method is that a growth modifier found to be effective for one zeolite might not be efficient for other frameworks. For example, the majority of the tested additives that changed the morphology of LTL crystals were found to have little influence on zeolite MOR having a similar structure [92]. To predict that an additive will provide an effective crystal shape modification is a big challenge. Molecular modeling could be a great approach to elucidate the possible binding modes on zeolite surfaces. However, one has to remember that it will be exceedingly complex to model every aspect of the zeolite synthesis gel chemistry.

1.4
Tools to Predict and Characterize Zeolite Morphology

In this section, we will discuss a few methods to predict and characterize zeolite morphology. Clearly, a wide array of methods is relevant such as sorption methods and spectroscopy. We do not intend to be exhaustive, but rather wish to highlight techniques that we believe hold a great potential for further advancement.

1.4.1
Computationally Guided Morphology Prediction

The use of computational methods to predict the effects of zeolite growth modifiers on the outcome of a zeolite synthesis has the potential to reduce or even completely remove any trial and error element of the procedure. The basis of such predictions should be a computer code doing molecular dynamics (MD). MD basically solves Newton's equations for each molecule in a simulation. It is a viable method for doing calculations when either the system's size exceeds thousands of atoms or when the number of simulations exceeds thousands.

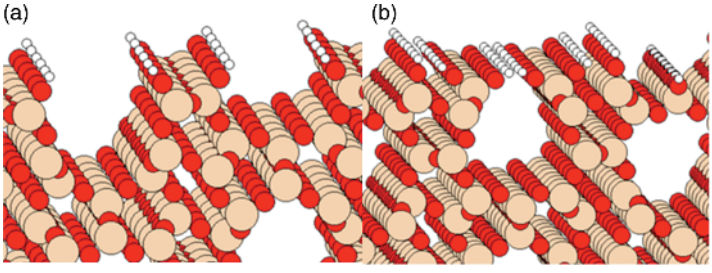

Figure 1.11 Two different ways of cleaving the same zeolite (MTT). (a) The resulting surface contains half pipe-like structures. (b) The surface is smooth.

However, only very recent literature addresses morphology control and prediction, and much work has to be done in order to arrive at a functional approach.

1.4.1.1 Predicting Zeolite Equilibrium Morphology

To predict the equilibrium morphology of a zeolite is the first step toward understanding the outcome of the synthesis. Even though the outcome of a synthesis procedure is not necessarily the equilibrium shape, this will give a basic understanding of the problem at hand. A suggested approach is to calculate the surface energy of the facets of the zeolite and use these energies to predict the equilibrium shape of the zeolite particle [110].

In order to calculate the surface energy of the facets, one needs to limit the amount of facets to investigate. In the literature, low-index Miller planes are often chosen. A zeolite has a large unit cell, thus a Miller plane is not one uniquely defined surface. This is in contrast to, for example, metals in an FCC structure where a Miller plane has a uniquely defined surface structure. A zeolite facet can have different surface structures; these are referred to as cleavings. To grasp this concept, the easiest example to consider is a 1D zeolite with straight channels. Considering a facet that is parallel with the channels, one could in a simple picture either cleave the zeolite through the channels, yielding a surface with half-pipes, or not through the channels, yielding a smoother and more homogenous surface (Figure 1.11).

Using MD, the energy of the chosen surface structures are calculated and the morphology can be predicted by a Wulff construction. A Wulff construction is a scheme of constructing a crystal in the equilibrium shape such that the surface Gibbs free energy is minimized [111]. This method has successfully predicted the shape of several zeolites, but cannot account for how the zeolite morphologies might depend on the synthesis procedure.

1.4.1.2 Modifier/Template Effect on Morphology

A method to predict the effect of the species-like templates and modifiers present in the synthesis gel is to analyze the behavior of these species when adsorbed at the zeolite surface. The same preparations regarding facets and cleavings as described in the preceding section are necessary. A suggested approach follows

these steps [112]: Try to insert the modifier molecule onto each surface. The most energetically favorable positions are then considered for each facet. If the modifier is strongly adsorbed in a position that will hinder or promote the growth on that facet, one can argue the qualitative effect of the modifier.

The effects of some species are most clearly interpreted if they are in a position to hinder growth. As an example, consider a chain-like modifier molecule, and again a 1D zeolite with straight channels. If the molecule adsorbs strongly perpendicular to the channels, it will retard the growth in that direction. However, if the molecule adsorbs along the channels, it might promote the growth in that direction, but it might also have no effect. This method is not quantifiable, so the detailed morphology cannot be predicted, but rather the qualitative effect can be speculated on. Nevertheless, this has successfully been done for the morphology effect of chain-like modifiers on some SAPO materials [112] and for crown ethers in zeolite L [113].

A drawback of the method is that it relies on an analysis of every single surface, and the possible positions of the species in question. From these analyses it is not always as easy to draw a conclusion as the simple example given here. The sheer number of possibilities makes it difficult to automate the method, hence making the screening of the morphology effect of many species tedious.

1.4.2 Structural Characterization of Zeolites by Transmission Electron Microscopy (TEM)

Electron microscopy (EM) is a very powerful technique for structural analysis at the nanometer scale, able to probe a very small area of the sample selectively. Using TEM it is possible to do both imaging and electron diffraction (ED) on the same region by adjusting the power of the lenses. Compared to the interaction with X-rays, where the scattering is caused by the electron density, the electrons from the beam are scattered by the electrostatic potential generated by both nucleus and electrons of the atoms. The interaction of electrons with matter is much stronger than with X-rays, allowing the measurement of very small crystals, but at the same time allowing multiple scattering especially for thick samples, allowing symmetry forbidden reflections to appear as weak spots. The intensities in ED are then caused by dynamical scattering. While this is not a problem for the phase identification or determination of the crystallographic orientation, it makes structure solution by direct methods impossible. A way to reduce the dynamical scattering is to use a very thin specimen or by rotating the tilted incident beam around the central axis, the so-called precession electron diffraction method (PED). By integrating the series of diffractograms collected at different precession angles, the intensities are semikinematical, allowing the use of direct methods; in such way in the recent past more zeolite structures have been solved with this method [114].

However, zeolites are extremely beam sensitive, and they suffer both radiolysis and knock-on displacement, so they can handle from 100 up to 10 000 times less radiation than other crystalline materials such as metals and metal oxides [115].

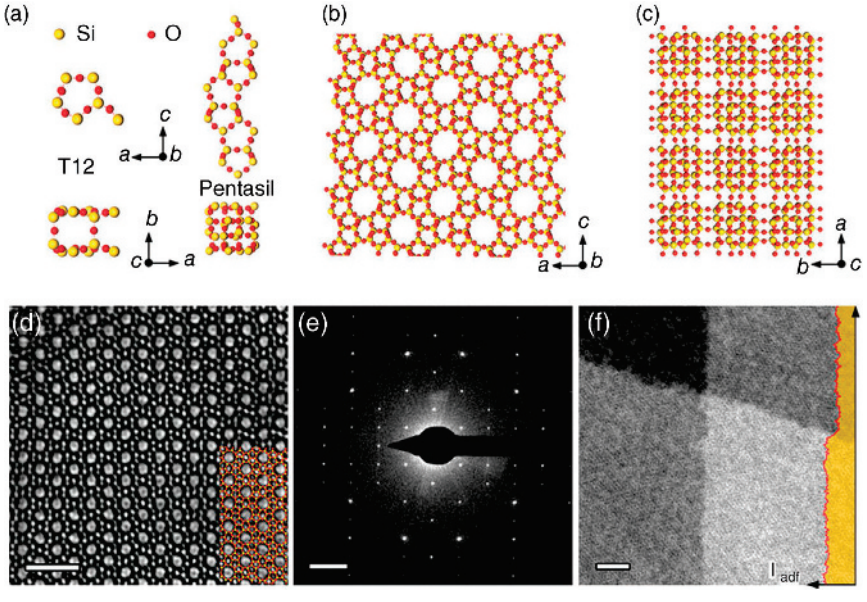

Figure 1.12 Structure (a–c) and electron micrograph and diffraction pattern (d–f) of two-dimensional nanosheet of ZSM-5. In part (d) is shown the micrograph of the crystal along [010] direction with the corresponding diffraction pattern (e) and structure (f) [117].

The experiments then need to be carried out in low-dose beam conditions, and the images are acquired at a dose-limited resolution [115]. For zeolite Y it has been observed that the higher the accelerating voltage, the better, and a higher Si/Al ratio allows the framework to tolerate a higher beam dose [116]. Figure 1.12 shows how TEM and ED can be used for structure identification and to determine how the topology is related to crystal morphology.

1.4.3
Powder XRD Anisotropic Peak Broadening Analysis for Morphology Investigations

Another useful and well-known technique used to study the morphology and size of nanocrystals is the analysis of the broadening of different peaks in XRD by using the well-known Scherrer equation:

$$L = \frac{K\lambda}{B \cdot \cos(\theta)},$$

where L is the crystallite average size; K is the shape factor, a dimensionless constant that can vary for different shape, with a value close to unit; λ is the X-ray wavelength; B is the peak width at half height; and θ is the diffracting angle (in radians).

Other sources of broadening such as crystal strain and instrument source sharpness need to be deconvoluted from the total peak broadening. To measure

the instrumental peak broadening, a typical procedure is to measure crystallites without strain in the size range 5–20 μm [118]. As the broadening caused by a routine instrument is usually in the range 0.08–0.2° [119], the size of the crystals can only be accurately estimated if less than 100–150 nm by this method.

A much more sophisticated analysis is achieved by selecting specific reflections; in particular the ones parallel to the crystallographic orientations h00 0k0 and 00l. By doing so, the average crystallite size along the three different crystallographic orientations of the crystal can be derived, and information about the total crystal morphology is revealed. For zeolite with very peculiar morphologies, such as the ZSM-5 nanosheets [89] with a thickness of only 2 unit cells, the anisotropic method has been applied successfully [120]. It was found that the average dimensions of an MFI nanosheet material were $29.8 \times 5.7 \times 37.8\,\text{nm}^3$ along the *a*-, *b*-, and *c*-axes, respectively. The great advantage of such measurements is that the values represent the whole sample or the average crystallite size, rather than a single or a few crystallites, as is often the case with microscopy.

1.5 Tailor-Made Catalysts for the Methanol-to-Hydrocarbons (MTH) Reaction

1.5.1 Introduction: The MTH Reaction – A Prime Example of Shape-Selective Nanocatalysis

In the early 1970s, about a decade after the introduction of the concept of shape-selective catalysis by Weisz and Frilette in the 1960s [121], workers at Mobil Research and Development Corporation made the remarkable discovery that methanol could be converted to high-quality gasoline over the zeolite ZSM-5. The concurrence of this discovery with the first oil crisis in 1973 led to a rapid development of a methanol-to-gasoline (MTG) process and its first large-scale commercialization in New Zealand in 1985 [122].

While the commercial activities have experienced considerable ups and downs in the following 30 years, the fundamental aspects of the transformation of methanol to hydrocarbons have remained a formidable scientific challenge and still today represent one of the most fascinating examples of shape-selective catalysis. Today, besides the conversion of MTG, methanol-to-olefins/propene (MTO and MTP) and methanol-to-aromatics (MTA) reactions are attracting interest. Many different zeolite topologies have been investigated, but interestingly the catalysts for all MTH processes have remained to be ZSM-5 and SAPO-34.

The aluminosilicate ZSM-5 zeolite has the MFI topology, characterized by a medium-sized three-dimensional pore structure. The pore system consists of interconnected straight ($5.1\,\text{Å} \times 5.5\,\text{Å}$) and zigzag ($5.3\,\text{Å} \times 5.6\,\text{Å}$) channels [123]. At the intersections slightly larger cavities are formed. The silicoaluminophosphate SAPO-34 zeotype has the CHA topology, composed of large cages that are

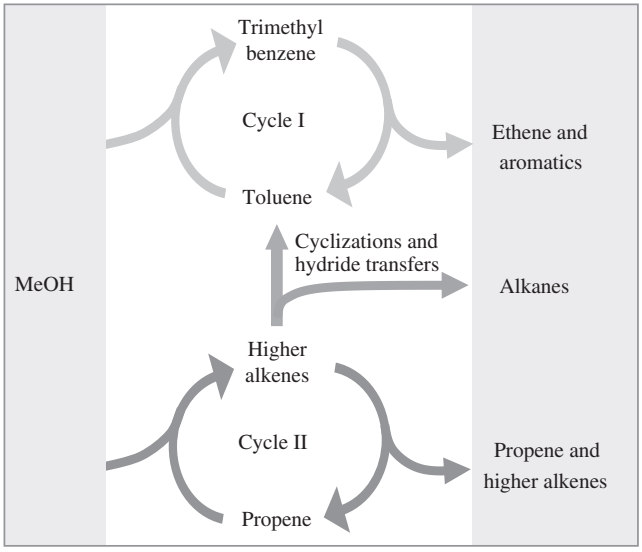

Figure 1.13 Dual cycle hydrocarbon pool mechanism. (Reprinted from Ref. [128] with permission from Elsevier.)

connected via small pore openings (3.8×3.8 Å) to form a three-dimensional system.

To understand the performance of zeolites in the MTH reaction it is useful to consider the hydrocarbon pool mechanism. This concept was coined by Dahl and Kolboe [124–126], and the mechanism was elaborated and further refined by Haw *et al.* [127]. In 2007, a breakthrough was made with the formulation of the dual cycle concept [128], which represents the current consensus (Figure 1.13).

The dual-cycle hydrocarbon pool mechanism consists of two cycles: (i) an alkene cycle in which alkenes are successively methylated until they reach a certain size and leave the zeolite pores again or they get cracked down to smaller sizes and reenter the catalytic cycle; (ii) an arene cycle in which aromatic molecules get methylated until they reach a certain size to either leave the zeolite pores or split smaller alkenes by molecular rearrangements and reenter the catalytic cycle. The cycles are linked when larger alkenes undergo cyclization accompanied by hydride transfer, resulting in the formation of aromatics and alkanes. Thus, the actual active site is an organic–inorganic hybrid species encapsulated within the subnanometer channels of the zeolite.

In ZSM-5, both cycles are operative and contribute to the reaction products. The pore sizes of ZSM-5 are large enough so that even tetramethylbenzenes can diffuse out of the zeolite crystals. Indeed, the product stream during MTH on ZSM-5 is typically rich in aromatic hydrocarbons (about 30 vol%) at intermediate reaction temperatures (320–420 °C). Therefore, ZSM-5 is the preferred zeolite for MTG applications. The dual cycle is also operative in SAPO-34, but the

small channels do not allow molecules larger than C_4 to diffuse out of the microporous network and it is difficult to separate reaction mechanism from diffusion. However, the large cages allow the retention of methylbenzenes, which are known to be active species to yield a product stream very rich in ethene and propene [129,130], and thus SAPO-34 is the preferred zeotype for MTO applications. However, it is important to stress that it is the interplay of topology, acid site density, and reaction conditions that ultimately determine the catalytic performance of a zeolite/zeotype material in the MTH reaction.

In the following sections we will establish a connection between the described possible synthetic approaches to modify the structural and textural properties of zeolites and their effects on the catalytic performance of the two archetype MTH catalysts ZSM-5 and SAPO-34.

1.5.2 Crystal Size Effects

The potent shape-selective properties of zeolites and zeotypes, caused by their crystalline microporous nature, result also in an inherent drawback of these materials, as molecules in nanosized channels experience severe diffusion limitations. Depending on crystal size and reaction conditions, it has been shown that only 10% of the acid sites in a zeolite may participate in the reactions in bulk crystals due to mass transfer limitations [12]. Therefore, diffusion of hydrocarbons is crucial to explain the reactivity and deactivation properties. The effectiveness factor (η) is the classical approach to measure the degree of catalyst utilization [131]. A full use of the catalyst is associated with a kinetically controlled regime with Thiele modulus (θ) close to zero and an effectiveness factor close to unity. In the case of diffusion-controlled regime, the Thiele modulus increases and the effectiveness factor decreases, leading to a poor use of the catalyst. Large crystals lead to higher diffusion limitations, larger Thiele modulus, and thus, less effective use of the zeolite (Figure 1.14). One way to overcome the diffusion limitations is the use of zeolite nanocrystals [89,120,132,133].

1.5.2.1 SAPO-34 (CHA-Topology)

As will become evident, a persistent challenge encountered throughout these sections is related to the ability to change only one catalyst parameter at a time, to carry out the genuine so-called single-parameter variations. Modifications of SAPO-34 crystals toward an average crystallite size in the nanometer range are naturally accompanied with an increased surface area. There is a clear benefit of the higher external surface area on the MTO lifetime for the nanosized SAPO-34 catalysts [134,135]. However, the stability of nanosized SAPO-34 when exposed to moisture at room conditions was found to be lower than that of the standard SAPO-34. Silicon content and distribution are also an important aspect that may control the selectivity and catalytic activity [136]. For example, if a synthesis method leading to nanocrystals also leads to a lower level of silicon

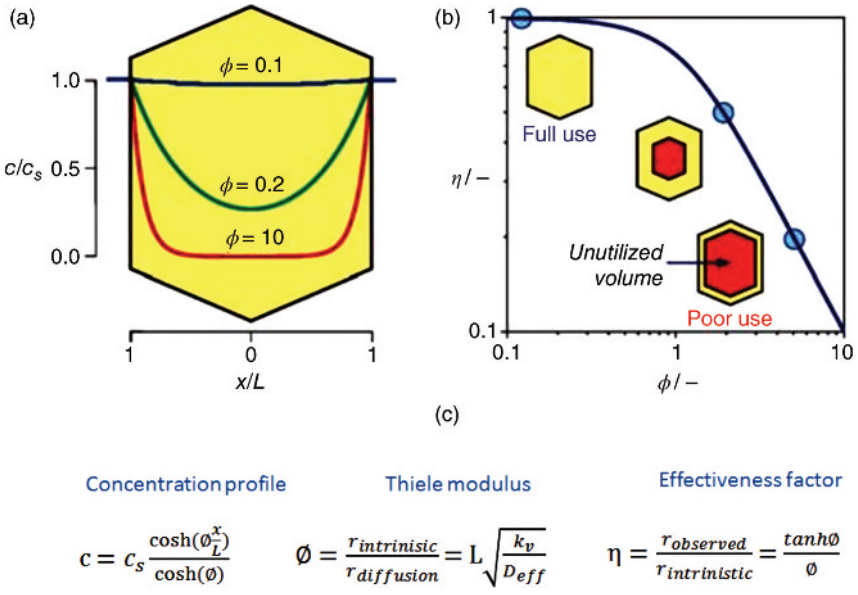

Figure 1.14 (a) Concentration profiles on a zeolite crystal with slab geometry at different Thiele modulus. (b) Effectiveness factor illustrating the use of the catalyst as a function of Thiele modulus. (c) Definition of concentration profile, Thiele modulus, and effectiveness factor. (Adapted from Ref. [12].)

incorporation, a slightly lower acidity is observed for the resulting catalysts, and any improved catalytic performance cannot be effectively attributed to the change in crystal size alone. Nevertheless, when acidity and crystal size are both varied, an increase in crystal size is found to have a greater impact on catalyst deactivation [135,137].

The deposition of large poly-aromatic species trapped in the nanocages of the SAPO-34 catalyst causes a reduction in the diffusivities. Reactants are prevented from reaching the acid sites and products cannot diffuse out the crystals. Internal mode of coke is responsible for the blocking of the catalyst pores and plays the most detrimental role. The formation of these polyaromatics has been linked to an increase in the ethene/propene ratio, which is generally seen with increasing deactivation [138]. Several studies have aimed at tuning the particle size of SAPO-34 and investigating the influence on the catalytic performance in the recent years. The general trend is that minimization of the crystallite size leads to longer lifetime [130,135,139–142]. Figure 1.15a–c shows SEM images of cubic crystals of SAPO-34 with different sizes. The improvement in lifetime when reducing the particle size from 8 to 1 µm can be observed in Figure 1.16 (traces (iv) and (iii)). Increased diffusion hindrance contributes not only to catalyst deactivation, but may also lead to a shift in product selectivity [130]. Small SAPO-34 crystals tend to lead to a higher initial propene/ethene ratio.

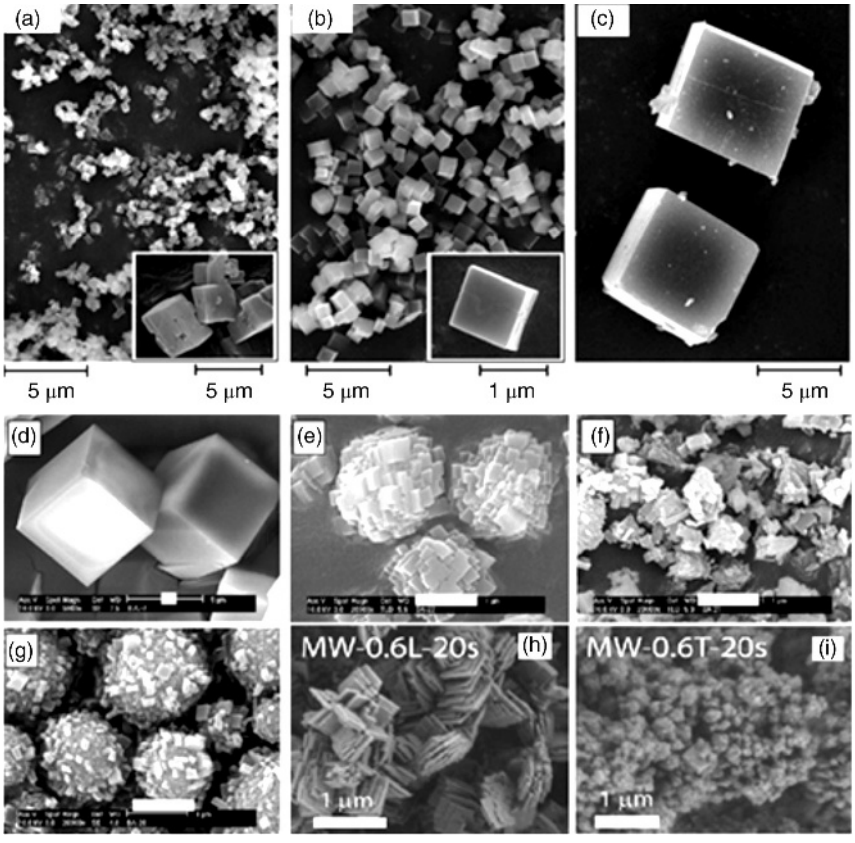

Figure 1.15 (a–c)Scanning electron micrographs of rhombohedral SAPO-34 particles of different sizes. (Adapted from Ref. [140].) (d–i) SEM images of the different SAPO-34 morphologies: cubic crystals (d), spherical aggregates of nanosized cubes (e), nanocrystals with irregular shape (f), spherical-shaped particles aggregated with SAPO-34 nanocrystals (g), nanosheets (h), and nanospheres (i). The white line indicates the size of 1 μm. (Adapted from Refs [134,137].)

Lee *et al.* studied how the crystal size variation of SAPO-34 catalyst affected their catalytic properties during MTH, and the different performance was attributed to the variations in the number of active accessible cages located near the external surface of the crystal. The fraction of active cages for the SAPO-34 with small crystals is higher than that of the catalyst with large crystallites (Figure 1.16b). Complementary explanations for the enhanced lifetime of small crystals refer to the lower diffusivity of product olefins into the SAPO-34 pores compared to that of methanol. The idea is that readsorption of the products is hindered, and therefore their subsequent reaction into coke is eliminated [139,141].

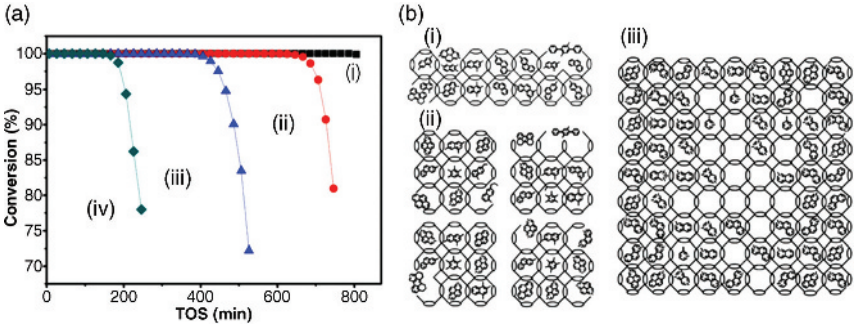

Figure 1.16 Methanol conversion variation with time-on-stream (a) and scheme of the coke location (b) over the SAPO-34 catalyst with different particle morphologies at 673 K and WHSV of 2 h–1: 20 nm × 250 nm × 250 nm (i), nanospheres 20–80 nm (ii), 1 μm cubic crystals (iii), and 8 μm cubic crystals (iv). (Adapted from Ref. [135].)

1.5.2.2 ZSM-5 (MFI Topology)

One of the first studies that attempts to correlate the crystal size of ZSM-5 zeolites and their catalytic properties for MTG was performed by Sugimoto *et al.* [143]. Two ZSM-5 samples with the smallest crystallites below 0.2 μm and the largest ones in the range of 3–4 μm were tested. The analysis of the product stream at full methanol conversion revealed higher selectivities toward C_{5+} hydrocarbons for the smaller crystals (64.2 versus 43.4 wt%), and a higher proportion of aromatics within the C_{5+} fraction (53.1 versus 23.0 wt%). The more facile formation of C_{5+} hydrocarbons was associated to the larger external surface area of the small crystals and therefore higher amounts of pore mouths. Additionally, the authors reported an equilibrium concentration of *p*-xylene within the xylenes isomers fraction of 26.1 wt% for the small crystals, whereas for the largest zeolite crystals a *p*-xylene selectivity of 83.1 wt% was observed, which they related to product shape selective properties of the large crystals. The isomerization reactions toward *p*-xylene dominate in the large crystals as *p*-xylene diffuses 1000 times faster than *o*- and *m*-xylenes. Deactivation was also linked to crystal size by Sugimoto *et al.* [143]. The small crystals retained larger amounts of carbon deposits, but their activity was higher after 100 h MTG reaction. The faster deactivation of the large crystals was then related to the blocking of the lower amounts of pore openings by coke.

Large ZSM-5 crystals have been also used to improve propylene formation during MTO reaction [144,145]. The behavior of conventional coffin-shaped crystals of around 5 μm was compared with large prismatic crystals around 15–20 μm. It was reported that the propene/ethene ratios were changed from 2–2.5 on the smaller crystals to 5.5 on the large crystals. However, the superior propylene production was ascribed to the combination of both the lower Brønsted acid sites and longer diffusion paths of the large crystals, illustrating well the challenges associated with performing single-parameter variations in zeolite catalysis.

1.5.3 Mesoporosity as Variable Parameter

Another method to shorten the diffusion path lengths and to increase the accessibility to the catalyst acid sites is to create an additional network of pores with different pore sizes connected to the micropore system. As already discussed in Section 1.2, postsynthesis alkali treatment and carbon templating are the most frequently used synthetic methods to introduce mesopores into ZSM-5 and SAPO-34. Generally, the observed effect on the MTH performance is similar as in the case of nanozeolites, as enhanced catalytic lifetime and reduction of the aromatic cycle are observed [67,146].

1.5.3.1 SAPO-34 (CHA Topology)

A number of synthesis strategies have been developed for making hierarchically nanoporous structures of the SAPO-34 zeotype catalyst. Longer catalytic lifetime is usually achieved when the additional pore system is introduced [54,147–149]. A slight increase in light olefin yield can be reached when accessible mesopores are created. However, it has been shown that hierarchical SAPO-34 systems synthesized using carbon nanoparticles or carbon nanotubes as templating agents had very different catalytic performance. Mesopores created by carbon nanoparticles were found to be located inside the particle without forming a three-dimensional mesopore network and thus did not enhance the catalyst lifetime, whereas a significant improvement in the conversion of methanol and catalyst stability was achieved with the open mesopores created within the nanotube-templated SAPO-34 catalyst. Besides, the additional pore system in the carbon nanotube-templated catalyst remained stable for a number of reactivation cycles, and it was additionally stable in terms of product distribution, which represents a key aspect for the industrial applications [147].

1.5.3.2 ZSM-5 (MFI Topology)

Ryoo and coworkers [19] performed a comparative study investigating the effect of mesoporosity against ZSM-5 deactivation during the MTH reaction. Different techniques for the creation of mesopores were applied. For hierarchical MFI samples, in which mesopores were created by alkaline treatment (BTZ sample in Figure 1.17) following the same conditions reported by Groen [29], the time to reach 50% of MeOH conversion was increased almost twofold in comparison to the purely microporous material (ZST sample in Figure 1.17). A very similar increase in lifetime was also achieved for ZSM-5 samples synthesized with carbon as template (CTZ sample in Figure 1.17).

Bjørgen *et al.* [18] investigated the influence of the alkaline concentration during desilication on the catalyst performance in the conversion of methanol to gasoline at 370 °C and ambient pressure. The conversion capacity was increased by a factor of 3.3 for the most severe treatment, while for a milder treatment the conversion capacity was improved by a factor of 2.4 with respect to the pristine ZSM-5 zeolite. In the same work, an increase in the initial activity as well as an

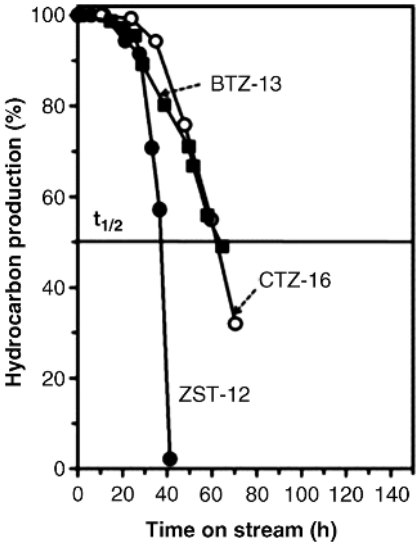

Figure 1.17 Catalyst lifetime for differently treated ZSM-5 catalysts, carbon-templated zeolite (CTZ-16), base-treated zeolite (BTZ-13), and pristine ZSM-5 (ZST-12). (Reprinted from Ref. [19] with permission from Elsevier.)

increase in the selectivity to the gasoline range C_{5+} products by a factor of 1.7 was observed over the whole MeOH conversion range for the best desilicated catalyst. Similar improvements were seen in more industrially relevant experiments carried out at 400 °C and 15 barg [20]. This clearly highlights the potential for catalyst and process improvement by this straightforward and affordable method. In a more fundamental study, Bleken *et al.* [41] compared the degree of deactivation of a commercial, purely microporous ZSM-5 to the desilicated version obtained using 0.3 M NaOH. It was concluded that the degree of deactivation in the desilicated sample was much more homogeneous than in the microporous sample. Also, the desilicated sample showed a similar coke distribution along the catalytic bed and could tolerate a larger amount of external coke than the regular sample.

1.5.4 Nanostructured Materials

1.5.4.1 SAPO-34 (CHA Topology)

Variations from the cubic shape of the typical SAPO-34 crystallite to other nanostructured morphologies will influence the performance in the MTO conversion [54,134–137,148]. Figure 1.15d–i shows SEM micrographs for the representative morphologies discussed in this section. As previously mentioned, both the (meso)pore system and acidity of the created structures are inherently affected when the morphology is modified. However, as was the case for particle

size, when different SAPO-34 morphologies are prepared with similar silicon environment distributions, the key factor for the improved catalytic lifetime is the length of the shortest diffusion pathway [150].

Starting from the rhombohedral micrometer-sized SAPO-34 particle, different templating methods lead to a change of the morphology toward spherical aggregates of nanosized SAPO-34 crystals (Figure 1.15) [134,135]. The activity and light olefin selectivity in the MTO reaction is hardly affected by the change in morphology when the acidity is unchanged. Nevertheless, an increase in lifetime from the original catalyst is effectively achieved. Different morphologies yield different extent of increase in lifetime. Investigations on the effect of different crystal morphologies with similar acidic properties on the MTO lifetime showed an optimum crystal size for spherical aggregates of nanosized cube-type SAPO-34 crystals with an average aggregate size of about 1 μm (Figure 1.16). Aminor increase in lifetime shown by SAPO-34 crystallites with irregular shape, where the surface of the spherical nanoparticles are aggregated with SAPO-34 nanocrystals, was attributed to too short diffusion lengths for the reaction intermediates to react to olefins within the crystals [134]. A nanosheet-like crystal morphology (Figure 1.15) is often obtained by microwave-assisted hydrothermal synthesis [135,137]. When comparing nanostructured SAPO-34 catalysts, the nanosheet-like crystals show the greatest increase in lifetime (Figure 1.16a). For a given coke content, a lower fraction of micropores are blocked by coke species deposited on the external crystal surface and thus, the accessibility of the reactants to the catalyst acid sites in the micropores is higher, maintaining higher MTO conversion for a longer time [137].

It has been so far evidenced that SAPO-34 crystals can be varied in different morphologies and sizes comprising micrometer-sized cubic crystals, nanospheres or aggregates, and nanosheet-like crystals, and their deactivation also occurs in different ways. In order to summarize the effect of the catalyst particle morphology in general, different deactivation modes are explained by means of the location of the retained coke species after methanol conversion for the three main crystal morphologies. Figure 1.16b presents the coke location and deactivation mode for the different SAPO-34 morphologies. For the crystals comprising cubic morphology on the micrometer range, the formation and accommodation of large aromatic molecules prevent methanol from accessing the active reaction site. Some cages in the central part of the SAPO-34 crystal particles experience no contact with methanol. Consequently, quick deactivation is observed over these bigger particles. For the nanosized crystal particles (nanospheres and nanosheets), most of the SAPO-34 cages are accessible during methanol conversion, and the usage of these nanosized catalysts is much more efficient. Simultaneously, quick escape of products also reduces the occurrence of hydrogen-transfer reactions and the formation of highly unsaturated products such as polycyclic aromatics (coke) [135,139]. Particularly, the nanosheet SAPO-34 catalyst presents the shortest diffusion lengths and also the lowest coking rate.

Only small changes can be observed in terms of MTO product selectivity. The high light olefin selectivity is maintained even when the size and morphology are

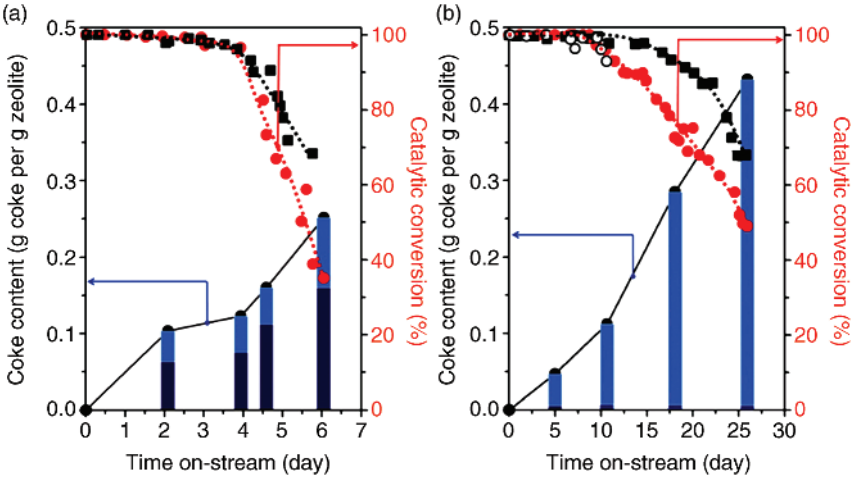

Figure 1.18 Conversion during MTH reaction versus time in stream and the amount of coke deposited on the zeolite (internal coke in dark blue, external coke in light blue). (a) Conventional MFI zeolite. (b) Unilamellar MFI zeolite. (Reprinted from Ref. [89] with permission from Nature Publishing Group.)

affected and very similar ethene-to-propene ratios are observed for the catalysts having different morphologies. A more severe coke deposition over the large SAPO-34 catalysts crystals leads to more ethene and less C_4–C_6 products, whereas the slight coke formation over nanosized catalysts has no substantial influence on the product diffusion, showing a relatively stable and high C_4–C_6 product selectivity.

1.5.4.2 ZSM-5 (MFI Topology)

As mentioned in Section 1.3.2, in groundbreaking work, Ryoo's group has created a novel family of zeolite materials by synthesizing nanolayered ZSM-5 with disordered and pillared structures [69,89] (see Figure 1.8) [89,151]. A significant improvement in lifetime in the MTH reaction was demonstrated and shown to be due to a lower coke deposition within the micropores of the nanostructured H-ZSM-5 zeolite (Figure 1.18). Despite the promise of long lifetime of the nanosheets materials, Bleken *et al.* [120] have indicated that the nanosheets have lower MTH activity than regular catalysts. By varying the contact time (WHSV) it was shown that the contact time needed to obtain the same conversion over nanosheets (2–3 nm thickness) was two times longer for the conventional crystals (0.5–3 μm). This was ascribed to the autocatalytic nature of the MTH reaction, as the more facile diffusion of the nanostructures countered the build-up of hydrocarbon pool species, which act as reaction centers [124,125]. In agreement, the MFI nanosheets exhibited higher aromatic yields and lower ethene production, reasonably due to the lower residence time of the aromatic hydrocarbons within the microporous structure of the sheets. It is accepted that

ethene is formed mainly by dealkylation of bulky polymethylbenzenes [152]. These species might diffuse more easily into the gas phase before dealkylation may occur for the nanosheets. We note that the improved diffusivity of hydrocarbons in MFI nanostructures makes this catalyst very attractive to be used as a model material for kinetic studies, hopefully avoiding the accumulation of hydrocarbons, which occurs in larger crystals.

Khare *et al.* [153] studied the MTH reaction using a series of ZSM-5 catalyst samples with different effective crystallite sizes, including also nanostructured materials and large crystals. The diffusion lengths were determined according to the crystal size and shape, and then correlated with the product selectivity during MTH reaction at 350 °C. The findings after 20 min on stream are reported in Figure 1.19. The ratio of (ethene)/(2-methylbutane and 2-methyl-2-butene) in the effluent was used as a descriptor to estimate the relative contribution of the alkene cycle and aromatics cycle [154]. It was observed that this ratio increases with the effective crystallite size, suggesting that the propagation of the aromatics cycle becomes more prominent with the increasing diffusion lengths. The increased intracrystalline residence time of polymethylbenzenes induced a higher hydrocarbon concentration inside the zeolite pores, leading to a larger extent of methylation and dealkylation reactions and therefore, producing more products of the aromatic-based cycle (aromatics and ethene) (Figure 1.19).

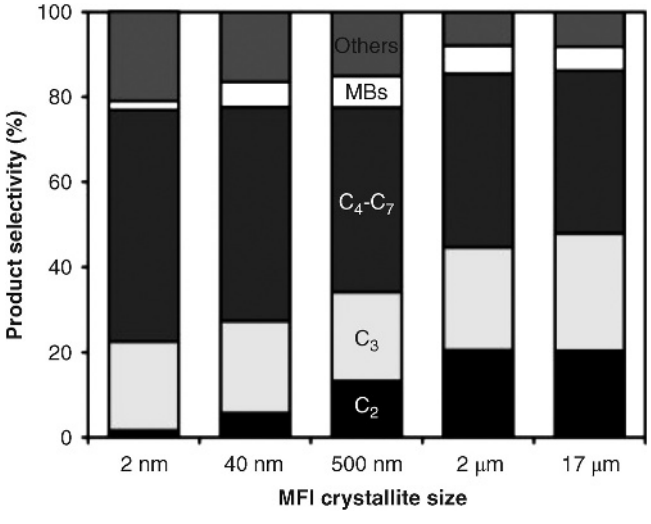

Figure 1.19 Selectivities on carbon basis during MTH by feeding DME over MFI crystals at 350 °C, 57–66 kPa DME partial pressure and 115–130 kPa total feed pressure, 46–59% net DME conversion, 20 min time on stream. (Reprinted from Ref. [153] with permission from Elsevier.)

1.6
Summary and Outlook

As is apparent from the preceding paragraphs, most of the literature that concerns the effect of zeolite particle nanostructure and morphology on the catalytic performance is essentially based on alterations of the access to or from the active sites by tuning *diffusion lengths*, either by creating mesopores, adjusting the particle size and shape, or by synthesizing layered materials by various methods. We will in this summarizing subsection outline a novel route to pursue in order to arrive at improved nanoporous zeolite catalysts that we believe hold great potential. Many zeolite topologies have pores of different sizes, which may be intersecting and of varying directionality. If intersecting pore systems of different sizes terminate and are exposed at different crystal facets, it will be possible to effectively force the products to leave the crystals via specific pore openings, if one is able to control the degree to which specific facets are exposed. In a recent patent [155] and journal publication [156], we have described a case where we utilize this idea. Due to a strongly preferred growth mechanism, certain crystal facets were indeed preferentially exposed, leading to a highly unexpected product shape selectivity. The results were obtained for zeolite SUZ-4 and are visualized in Figure 1.20. As the material prefers to crystallize as needles, the 10-ring channels running along the *c*-direction (the direction of the needles) will only be

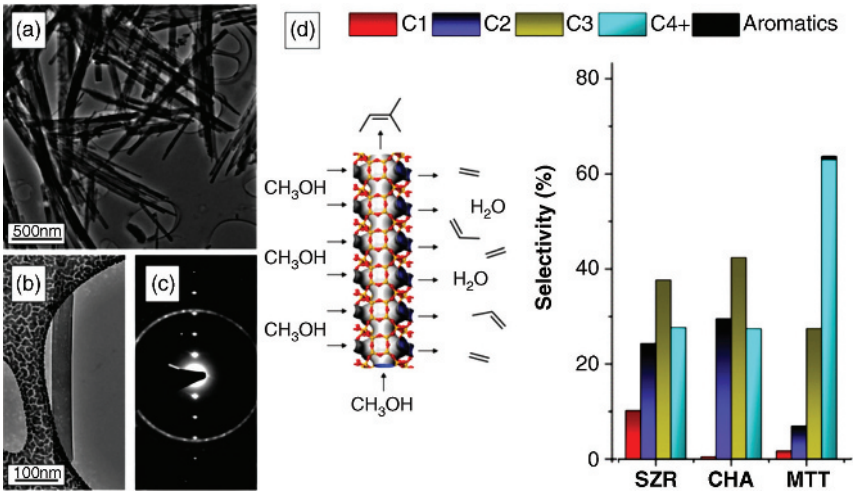

Figure 1.20 *Right panel:* Product selectivity in the methanol to hydrocarbons reaction. Zeolite SZR behaves like the archetype 8-ring material CHA, despite the presence of 10-rings. Typical 10-ring selectivities are shown for zeolite MTT. Panels (a) and (b) show the needle-like morphology (SEM and TEM), and the diffraction (c) proves that the 8-rings cover the side of the needles, thus determining the product selectivity for this morphology, and that the 10-rings are only accessible from the ends of the needles (d) [155,156].

exposed to the gas phase via the ends of the needles, whereas the 8-ring channels running perpendicular to the *c*-direction are exposed to the surroundings on the majority of the crystal surface. Thus, the material displays shape selective properties like an 8-ring zeolite despite the presence of 10-rings and the shape selectivity is determined primarily by particle morphology and not framework topology.

During our systematic investigations of zeolite catalysts comprising pore channels of different dimensions (e.g., 8- and 10-rings) [157,158], we realized that this might be a general feature, that is, it could be possible to tune the shape selectivity and properties of nanoporous materials by altering the particle morphology so that different facets where different channel systems terminate are preferentially exposed. The idea outlined here constitutes a new perspective on how to influence the properties of nanoporous materials. The effects of preferential exposure of certain crystal facets are well documented within other areas of catalysis and materials science, such as nanoparticle-based catalysis, but appears to have received much less attention within zeolite catalysis, presumably because the properties of nanoporous materials are generally linked to the internal rather than external surface, whereas the properties of, for example, metal nanoparticles or functional oxides are obviously linked to the external surfaces. We strongly believe that it will be possible to systematically tune the performance of nanoporous materials as catalysts and adsorbents by controlling the exposure of specific crystal facets, as indicated here. This could be a highly rewarding and completely new research direction for developing nanoporous materials with improved properties.

Acknowledgments

Financial support is received via the European Industrial Doctorates project "ZeoMorph" (Grant Agreement No. 606965), part of the Marie Curie actions (FP7-PEOPLE-2013-ITN-EID). The authors thank Dr. Lukasz Mentel for contributing Figure 1.7.

References

1 Corma, A. and Martinez, A. (1995) Zeolites and zeotypes as catalysts. *Adv. Mater.*, **7**, 137–144.
2 Nascimento, M.A.C. (2001) *Theoretical Aspects of Heterogeneous Catalysis*, Kluwer Academic Publishers, Dordrecht, Germany.
3 Moliner, M., Martínez, C., and Corma, A. (2015) Multipore zeolites: synthesis and catalytic applications. *Angew. Chem., Int. Ed.*, **54**, 3560–3579.
4 Cundy, C.S. and Cox, P.A. (2003) The hydrothermal synthesis of zeolites: history and development from the earliest days to the present time. *Chem. Rev.*, **103**, 663–701.
5 Wilson, S.T., Lok, B.M., Messina, C.A., Cannan, T.R., and Flanigen, E.M. (1982) Aluminophosphate molecular sieves: a new class of microporous crystalline inorganic solids. *J. Am. Chem. Soc.*, **104**, 1146–1147.

6 Rocha, J. and Anderson, M.W. (2000) Microporous titanosilicates and other novel mixed octahedral–tetrahedral framework oxides. *Eur. J. Inorg. Chem.*, **2000**, 801–818.

7 Serrano, D.P. and van Grieken, R. (2001) Heterogenous events in the crystallization of zeolites. *J. Mater. Chem.*, **11**, 2391–2407.

8 Cundy, C.S. and Cox, P.A. (2005) The hydrothermal synthesis of zeolites: precursors, intermediates and reaction mechanism. *Microporous Mesoporous Mater.*, **82**, 1–78.

9 Roth, W.J. (2007) Synthesis of delaminated and pillared zeolitic materials, in *Studies in Surface Science and Catalysis* (eds J. Čejka, H. van Bekkum, A. Corma, and F. Schüth), Elsevier, pp. 221–239.

10 Yu, J. (2007) Synthesis of zeolites, in *Studies in Surface Science and Catalysis* (eds J. Čejka, H. van Bekkum, A. Corma, and F. Schüth), Elsevier, pp. 39–103.

11 Zhao, D. and Wan, Y. (2007) The synthesis of mesoporous molecular sieves, in *Studies in Surface Science and Catalysis* (eds J. Čejka, H. van Bekkum, A. Corma, and F. Schüth), Elsevier, pp. 241 III.

12 Pérez-Ramírez, J., Christensen, C.H., Egeblad, K., Christensen, C.H., and Groen, J.C. (2008) Hierarchical zeolites: enhanced utilisation of microporous crystals in catalysis by advances in materials design. *Chem. Soc. Rev.*, **37**, 2530–2542.

13 Ogura, M., Shinomiya, S.Y., Tateno, J., Nara, Y., Kikuchi, E., and Matsukata, M. (2000) Formation of uniform mesopores in ZSM-5 zeolite through treatment in alkaline solution. *Chem. Lett.*, **29**, 882–883.

14 Groen, J.C., Peffer, L.A.A., Moulijn, J.A., and Pérez-Ramírez, J. (2004) Mesoporosity development in ZSM-5 zeolite upon optimized desilication conditions in alkaline medium. *Colloids Surf. A*, **241**, 53–58.

15 Ogura, M., Shinomiya, S.Y., Tateno, J., Nara, Y., Nomura, M., Kikuchi, E., and Matsukata, M. (2001) Alkali-treatment technique: new method for modification of structural and acid-catalytic properties of ZSM-5 zeolites. *Appl. Catal. A*, **219**, 33–43.

16 Groen, J.C., Moulijn, J.A., and Pérez-Ramírez, J. (2005) Decoupling mesoporosity formation and acidity modification in ZSM-5 zeolites by sequential desilication–dealumination. *Microporous Mesoporous Mater.*, **87**, 153–161.

17 Groen, J.C., Moulijn, J.A., and Perez-Ramirez, J. (2006) Desilication: on the controlled generation of mesoporosity in MFI zeolites. *J. Mater. Chem.*, **16**, 2121–2131.

18 Bjørgen, M., Joensen, F., Holm, M.S., Olsbye, U., Lillerud, K.-P., and Svelle, S. (2008) Methanol to gasoline over zeolite H-ZSM-5: improved catalyst performance by treatment with NaOH. *Appl. Catal. A*, **345**, 43–50.

19 Kim, J., Choi, M., and Ryoo, R. (2010) Effect of mesoporosity against the deactivation of MFI zeolite catalyst during the methanol-to-hydrocarbon conversion process. *J. Catal.*, **269**, 219–228.

20 Svelle, S., Sommer, L., Barbera, K., Vennestrøm, P.N.R., Olsbye, U., Lillerud, K.P., Bordiga, S., Pan, Y.-H., and Beato, P. (2011) How defects and crystal morphology control the effects of desilication. *Catal. Today*, **168**, 38–47.

21 Corma, A., Martinez, C., and Doskocil, E. (2013) Designing MFI-based catalysts with improved catalyst life for $C = 3$ and $C = 5$ oligomerization to high-quality liquid fuels. *J. Catal.*, **300**, 183–196.

22 Beato, P. (2010) Process for converting oxygenates to hydrocarbons. Google Patents.

23 Groen, J.C., Zhu, W., Brouwer, S., Huynink, S.J., Kapteijn, F., Moulijn, J.A., and Pérez-Ramírez, J. (2007) Direct demonstration of enhanced diffusion in mesoporous ZSM-5 zeolite obtained via controlled desilication. *J. Am. Chem. Soc.*, **129**, 355–360.

24 Abelló, S., Bonilla, A., and Pérez-Ramírez, J. (2009) Mesoporous ZSM-5 zeolite catalysts prepared by desilication with organic hydroxides and comparison with

NaOH leaching. *Appl. Catal. A*, **364**, 191–198.

25 Fernandez, C., Stan, I., Gilson, J.P., Thomas, K., Vicente, A., Bonilla, A., and Pérez-Ramírez, J. (2010) Hierarchical ZSM-5 zeolites in shape-selective xylene isomerization: role of mesoporosity and acid site speciation. *Chem. Eur. J.*, **16**, 6224–6233.

26 Holm, M.S., Egeblad, K., Vennestrøm, P.N.R., Hartmann, C.G., Kustova, M., and Christensen, C.H. (2008) Enhancing the porosity of mesoporous carbon-templated ZSM-5 by desilication. *Eur. J. Inorg. Chem.*, **2008**, 5185–5189.

27 Milina, M., Mitchell, S., Cooke, D., Crivelli, P., and Pérez-Ramírez, J. (2015) Impact of pore connectivity on the design of long-lived zeolite catalysts. *Angew. Chem., Int. Ed.*, **54**, 1591–1594.

28 Groen, J.C., Bach, T., Ziese, U., Paulaime-Van Donk, A.M., De Jong, K.P., Moulijn, J.A., and Pérez-Ramírez, J. (2005) Creation of hollow zeolite architectures by controlled desilication of A1-zoned ZSM-5 crystals. *J. Am. Chem. Soc.*, **127**, 10792–10793.

29 Groen, J.C., Jansen, J.C., Moulijn, J.A., and Pérez-Ramírez, J. (2004) Optimal aluminum-assisted mesoporosity development in MFI zeolites by desilication. *J. Phys. Chem. B*, **108**, 13062–13065.

30 Possato, L.G., Diniz, R.N., Garetto, T., Pulcinelli, S.H., Santilli, C.V., and Martins, L. (2013) A comparative study of glycerol dehydration catalyzed by micro/mesoporous MFI zeolites. *J. Catal.*, **300**, 102–112.

31 Yu, W., Deng, L., Yuan, P., Liu, D., Yuan, W., and Chen, F. (2015) Preparation of hierarchically porous diatomite/MFI-type zeolite composites and their performance for benzene adsorption: the effects of desilication. *Chem. Eng. J.*, **270**, 450–458.

32 Mitchell, S., Milina, M., Verel, R., Hernandez-Rodriguez, M., Perez-Ramirez, J., Pinar, A.B., and McCusker, L.B. (2015) Aluminum redistribution during the preparation of hierarchical zeolites by desilication. *Chin. J. Chem.*, **21**, 14156–14164.

33 Jung, J., Jo, C., Mota, F.M., Cho, J., and Ryoo, R. (2015) Acid catalytic function of mesopore walls generated by MFI zeolite desilication in comparison with external surfaces of MFI zeolite nanosheet. *Appl. Catal. A*, **492**, 68–75.

34 Verboekend, D., Mitchell, S., Milina, M., Groen, J.C., and Perez-Ramirez, J. (2011) Full compositional flexibility in the preparation of mesoporous MFI zeolites by desilication. *J. Phys. Chem. C*, **115**, 14193–14203.

35 Suzuki, T. and Okuhara, T. (2001) Change in pore structure of MFI zeolite by treatment with NaOH aqueous solution. *Microporous Mesoporous Mater.*, **43**, 83–89.

36 Su, L., Liu, L., Zhuang, J., Wang, H., Li, Y., Shen, W., Xu, Y., and Bao, X. (2003) Creating mesopores in ZSM-5 zeolite by alkali treatment: a new way to enhance the catalytic performance of methane dehydroaromatization on Mo/HZSM-5 catalysts. *Catal. Lett.*, **91**, 155–167.

37 Mitchell, S., Michels, N.-L., Kunze, K., and Perez-Ramirez, J. (2012) Visualization of hierarchically structured zeolite bodies from macro to nano length scales. *Nat. Chem.*, **4**, 825–831.

38 Perez-Ramirez, J., Verboekend, D., Bonilla, A., and Abello, S. (2009) Zeolite catalysts with tunable hierarchy factor by pore-growth moderators. *Adv. Funct. Mater.*, **19**, 3972–3979.

39 Čimek, A., Subotić, B., Šmit, I., Tonejc, A., Aiello, R., Crea, F., and Nastro, A. (1997) Dissolution of high-silica zeolites in alkaline solutions II. Dissolution of 'activated' silicalite-1 and ZSM-5 with different aluminum content. *Microporous Mater.*, **8**, 159–169.

40 Caicedo-Realpe, R. and Pérez-Ramírez, J. (2010) Mesoporous ZSM-5 zeolites prepared by a two-step route comprising sodium aluminate and acid treatments. *Microporous Mesoporous Mater.*, **128**, 91–100.

41 Bleken, F.L., Barbera, K., Bonino, F., Olsbye, U., Lillerud, K.P., Bordiga, S., Beato, P., Janssens, T.V.W., and Svelle, S. (2013) Catalyst deactivation by coke formation in microporous and desilicated zeolite H-ZSM-5 during the conversion

of methanol to hydrocarbons. *J. Catal.*, **307**, 62–73.

42 Fathi, S., Sohrabi, M., and Falamaki, C. (2014) Improvement of HZSM-5 performance by alkaline treatments: comparative catalytic study in the MTG reactions. *Fuel*, **116**, 529–537.

43 Gil, B., Mokrzycki, L., Sulikowski, B., Olejniczak, Z., and Walas, S. (2010) Desilication of ZSM-5 and ZSM-12 zeolites: impact on textural, acidic and catalytic properties. *Catal. Today*, **152**, 24–32.

44 Gopalakrishnan, S., Zampieri, A., and Schwieger, W. (2008) Mesoporous ZSM-5 zeolites via alkali treatment for the direct hydroxylation of benzene to phenol with N_2O. *J. Catal.*, **260**, 193–197.

45 Groen, J.C., Peffer, L.A.A., Moulijn, J.A., and Perez-Ramirez, J. (2005) Mechanism of hierarchical porosity development in MFI zeolites by desilication: the role of aluminum as a pore-directing agent. *Chem. Eur. J.*, **11**, 4983–4994.

46 Jong, K.P., Zečević, J., Friedrich, H., de Jongh, P.E., Bulut, M., van Donk, S., Kenmogne, R., Finiels, A., Hulea, V., and Fajula, F. (2010) Zeolite Y crystals with trimodal porosity as ideal hydrocracking catalysts. *Angew. Chem.*, **122**, 10272–10276.

47 Sommer, L., Mores, D., Svelle, S., Stöcker, M., Weckhuysen, B.M., and Olsbye, U. (2010) Mesopore formation in zeolite H-SSZ-13 by desilication with NaOH. *Microporous Mesoporous Mater.*, **132**, 384–394.

48 Groen, J.C., Abelló, S., Villaescusa, L.A., and Pérez-Ramírez, J. (2008) Mesoporous beta zeolite obtained by desilication. *Microporous Mesoporous Mater.*, **114**, 93–102.

49 Groen, J.C., Peffer, L.A.A., Moulijn, J.A., and Perez-Ramirez, J. (2004) On the introduction of intracrystalline mesoporosity in zeolites upon desilication in alkaline medium. *Microporous Mesoporous Mater.*, **69**, 29–34.

50 Jin, Y., Xiao, C., Liu, J., Zhang, S., Asaoka, S., and Zhao, S. (2015) Mesopore modification of beta zeolites by sequential alkali and acid treatments: narrowing mesopore size distribution featuring unimodality and mesoporous texture properties estimated upon a mesoporous volumetric model. *Microporous Mesoporous Mater.*, **218**, 180–191.

51 Verboekend, D., Vilé, G., and Pérez-Ramírez, J. (2012) Mesopore formation in USY and beta zeolites by base leaching: selection criteria and optimization of pore-directing agents. *Cryst. Growth Des.*, **12**, 3123–3132.

52 Holm, M.S., Hansen, M.K., and Christensen, C.H. (2009) "One-pot" ion-exchange and mesopore formation during desilication. *Eur. J. Inorg. Chem.*, **2009**, 1194–1198.

53 Pérez-Ramírez, J., Abelló, S., Bonilla, A., and Groen, J.C. (2009) Tailored mesoporosity development in zeolite crystals by partial detemplation and desilication. *Adv. Funct. Mater.*, **19**, 164–172.

54 Wang, L., Xiao, C., Liu, J., Zhang, S., Feng, R., and Jin, Y. (2015) Effects of alkali and acid modification treatments method on size distribution and textural property of β zeolites. *Shiyou Huagong/Petrochem. Technol.*, **44**, 839–845.

55 Bonilla, A., Baudouin, D., and Pérez-Ramírez, J. (2009) Desilication of ferrierite zeolite for porosity generation and improved effectiveness in polyethylene pyrolysis. *J. Catal.*, **265**, 170–180.

56 Mokrzycki, Ł., Sulikowski, B., and Olejniczak, Z. (2009) Properties of desilicated ZSM-5, ZSM-12, MCM-22 and ZSM-12/MCM-41 derivatives in isomerization of α-pinene. *Catal. Lett.*, **127**, 296–303.

57 Wei, X. and Smirniotis, P.G. (2006) Development and characterization of mesoporosity in ZSM-12 by desilication. *Microporous Mesoporous Mater.*, **97**, 97–106.

58 van Laak, A.N.C., Sagala, S.L., Zečević, J., Friedrich, H., de Jongh, P.E., and de Jong, K.P. (2010) Mesoporous mordenites obtained by sequential acid and alkaline treatments: catalysts for cumene

production with enhanced accessibility. *J. Catal.*, **276**, 170–180.

59 Groen, J.C., Peffer, L.A.A., Moulijn, J.A., and Pérez, R.J. (2004) On the introduction of intracrystalline mesoporosity in zeolites upon desilication in alkaline medium. *Microporous Mesoporous Mater.*, **69**, 29–34.

60 Huang, S., Liu, X., Yu, L., Miao, S., Liu, Z., Zhang, S., Xie, S., and Xu, L. (2014) Preparation of hierarchical mordenite zeolites by sequential steaming-acid leaching-alkaline treatment. *Microporous Mesoporous Mater.*, **191**, 18–26.

61 Paixão, V., Carvalho, A.P., Rocha, J., Fernandes, A., and Martins, A. (2010) Modification of MOR by desilication treatments: structural, textural and acidic characterization. *Microporous Mesoporous Mater.*, **131**, 350–357.

62 Macedo, H.P., de Oliveira Felipe, L.C., Silva, L.B., Garcia, L.M.P., Medeiros, R.L.B.A., and Costa, T.R. (2014) Application of design of experiments to the alkaline treatment in mordenite zeolite: influence on Si/Al ratio. *Mater. Sci. Forum.*, **798–799**, pp. 435–442.

63 Verboekend, D., Chabaneix, A.M., Thomas, K., Gilson, J.-P., and Perez-Ramirez, J. (2011) Mesoporous ZSM-22 zeolite obtained by desilication: peculiarities associated with crystal morphology and aluminium distribution. *CrystEngComm*, **13**, 3408–3416.

64 Qin, Z., Shen, B., Gao, X., Lin, F., Wang, B., and Xu, C. (2011) Mesoporous Y zeolite with homogeneous aluminum distribution obtained by sequential desilication–dealumination and its performance in the catalytic cracking of cumene and 1,3,5-triisopropylbenzene. *J. Catal.*, **278**, 266–275.

65 Martens, J.A., Verboekend, D., Thomas, K., Vanbutsele, G., Gilson, J.-P., and Perez-Ramirez, J. (2013) Hydroisomerization of emerging renewable hydrocarbons using hierarchical Pt/H-ZSM-22 catalyst. *Sustain. Green Chem.*, **6**, 421–425.

66 Matias, P., Sa, C.C., Graca, I., Lopes, J.M., Carvalho, A.P., Ramoa, R.F., and Guisnet, M. (2011) Desilication of a TON zeolite with NaOH: influence on porosity, acidity and catalytic properties. *Appl. Catal. A*, **399**, 100–109.

67 del. Campo, P., Slawinski, W.A., Henry, R., Erichsen, M.W., Svelle, S., Beato, P., Wragg, D., and Olsbye, U. (2015) Time- and space-resolved high energy operando X-ray diffraction for monitoring the methanol to hydrocarbon reaction over H-ZSM-22 zeolite catalyst in different conditions. *Surf. Sci.*, **648**, 141–149.

68 Li, Y., Liu, S., Zhang, Z., Xie, S., Zhu, X., and Xu, L. (2008) Aromatization and isomerization of 1-hexene over alkali-treated HZSM-5 zeolites: improved reaction stability. *Appl. Catal. A*, **338**, 100–113.

69 Musilová-Pavlačková, Z., Zones, S., and Čejka, J. (2010) Post-synthesis modification of SSZ-35 zeolite to enhance the selectivity in *p*-xylene alkylation with isopropyl alcohol. *Top. Catal.*, **53**, 273–282.

70 Pérez-Ramírez, J., Abelló, S., Villaescusa, L.A., and Bonilla, A. (2008) Toward functional clathrasils: size- and composition-controlled octadecasil nanocrystals by desilication. *Angew. Chem., Int. Ed.*, **47**, 7913–7917.

71 Kubů, M., Žilková, N., and Čejka, J. (2011) Post-synthesis modification of TUN zeolite: textural, acidic and catalytic properties. *Catal. Today*, **168**, 63–70.

72 Schwieger, W., Machoke, A.G., Weissenberger, T., Inayat, A., Selvam, T., Klumpp, M., and Inayat, A. (2016) Hierarchy concepts: classification and preparation strategies for zeolite containing materials with hierarchical porosity. *Chem. Soc. Rev.*

73 Jacobsen, C.J.H., Madsen, C., Houzvicka, J., Schmidt, I., and Carlsson, A. (2000) Mesoporous zeolite single crystals. *J. Am. Chem. Soc.*, **122**, 7116–7117.

74 Schmidt, I., Boisen, A., Gustavsson, E., Ståhl, K., Pehrson, S., Dahl, S., Carlsson, A., and Jacobsen, C.J.H. (2001) Carbon nanotube templated growth of mesoporous zeolite single crystals. *Chem. Mater.*, **13**, 4416–4418.

75 Pérez-Pariente, J. and Álvaro-Muñoz, T. (2015) Strategies to improve the accessibility to the intracrystalline void of

zeolite materials: some chemical reflection, in *Mesoporous Zeolites*, Wiley-VCH Verlag GmbH, Weinheim, Germany, pp. 1–30.
76 Renzo, F.D. (1998) Zeolites as tailor-made catalysts: control of the crystal size. *Catal. Today*, **41**, 37–40.
77 Evgeny, M.J.M.M., Rebrov, V., de Croon, M.H.J.M., and Schouten, J.C. (2009) Hydrothermal synthesis of zeolitic coatings for applications in microstructured reactors, in *Ordered Porous Solids*, Elsevier.
78 Vuong, G.-T. and Do, T.-O. (2009) Synthesis of silylated nanozeolites in the presence of organic phase: two-phase and single-phase methods. *Microporous Mesoporous Mater.*, **120**, 310–316.
79 Vuong, G.-T. and Do, T.-O. (2007) A new route for the synthesis of uniform nanozeolites with hydrophobic external surface in organic solvent medium. *J. Am. Chem. Soc.*, **129**, 3810–3811.
80 Serrano, D.P., Aguado, J., Escola, J.M., Rodríguez, J.M., and Peral, Á. (2006) Hierarchical zeolites with enhanced textural and catalytic properties synthesized from organofunctionalized seeds. *Chem. Mater.*, **18**, 2462–2464.
81 Serrano, D.P., Aguado, J., Morales, G., Rodríguez, J.M., Peral, A., Thommes, M., Epping, J.D., and Chmelka, B.F. (2009) Molecular and meso- and macroscopic properties of hierarchical nanocrystalline ZSM-5 zeolite prepared by seed silanization. *Chem. Mater.*, **21**, 641–654.
82 Serrano, D.P., Aguado, J., Escola, J.M., Peral, A., Morales, G., and Abella, E. (2011) Synthesis of hierarchical ZSM-5 by silanization and alkoxylation of protozeolitic units. *Catal. Today*, **168**, 86–95.
83 Lawton, S.L., Fung, A.S., Kennedy, G.J., Alemany, L.B., Chang, C.D., Hatzikos, G.H., Lissy, D.N., Rubin, M.K., Timken, H.-K.C., Steuernagel, S., and Woessner, D.E. (1996) Zeolite MCM-49: a three-dimensional MCM-22 analogue synthesized by *in situ* crystallization. *J. Phys. Chem.*, **100**, 3788–3798.
84 Chlubná, P., Roth, W.J., Zukal, A., Kubů, M., and Pavlatová, J. (2012) Pillared MWW zeolites MCM-36 prepared by swelling MCM-22P in concentrated surfactant solutions. *Catal. Today*, **179**, 35–42.
85 Corma, A., Fornés, V., Guil, J.M., Pergher, S., Maesen, T.L.M., and Buglass, J.G. (2000) Preparation, characterisation and catalytic activity of ITQ-2, a delaminated zeolite. *Microporous Mesoporous Mater.*, **38**, 301–309.
86 Pastore, H.O. and Cardoso, D. (2015) *Zeolite Structures of Nanometer Morphology: Small Dimensions, New Possibilities*, Wiley-VCH Verlag GmbH, Weinheim, Germany.
87 Roth, W.J., Gil, B., Makowski, W., Marszalek, B., and Eliasova, P. (2016) Layer like porous materials with hierarchical structure. *Chem. Soc. Rev*, **45**, 3400–3438.
88 Roth, W.J., Nachtigall, P., Morris, R.E., and Čejka, J. (2014) Two-dimensional zeolites: current status and perspectives. *Chem. Rev.*, **114**, 4807–4837.
89 Choi, M., Na, K., Kim, J., Sakamoto, Y., Terasaki, O., and Ryoo, R. (2009) Stable single-unit-cell nanosheets of zeolite MFI as active and long-lived catalysts. *Nature*, **461**, 246–249.
90 Na, C.J.K., Kim, J., Cho, K., Jung, J., Seo, R.J.M.Y., Chmelka, B.F., and Ryoo, R. Directing zeolite structures into hierarchically nanoporous architectures. *Supramol. Sci.*, **333**, 328–332.
91 Möller, K. and Bein, T. (2011) Pores within pores: how to craft ordered hierarchical zeolites. *Supramol. Sci.*, **333**, 297–298.
92 Rimer, J.D., Kumar, M., Li, R., Lupulescu, A.I., and Oleksiak, M.D. (2014) Tailoring the physicochemical properties of zeolite catalysts. *Catal. Sci. Tech.*, **4**, 3762–3771.
93 Choi, K.-S. (2008) Shape control of inorganic materials via electrodeposition. *Dalton Trans.*, 5432–5438.
94 Addadi, L., Berkovitch-Yellin, Z., Domb, N., Gati, E., Lahav, M., and Leiserowitz, L. (1982) Resolution of conglomerates by stereoselective habit modifications. *Nature*, **296**, 21–26.
95 Sano, T., Wakabayashi, S., Oumi, Y., and Uozumi, T. (2001) Synthesis of large mordenite crystals in the presence of

aliphatic alcohol. *Microporous Mesoporous Mater.*, **46**, 67–74.
96 Gomez, A.G., Silveira, G.D., Doan, H., and Cheng, C.-H. (2011) A facile method to tune zeolite L crystals with low aspect ratio. *Chem. Commun.*, **47**, 5876–5878.
97 Lupulescu, A.I., Kumar, M., and Rimer, J.D. (2013) A facile strategy to design zeolite L crystals with tunable morphology and surface architecture. *J. Am. Chem. Soc.*, **135**, 6608–6617.
98 Jamil, A.K., Muraza, O., and Al-Amer, A.M. (2015) The role of alcohols and diols as co-solvents in fabrication of TON zeolite. *J. Ind. Eng. Chem.*, **29**, 112–119.
99 Gaona-Gómez, A. and Cheng, C.-H. (2012) Modification of zeolite L (LTL) morphology using diols, $(OH)_2(CH_2)_{2n+2}O_n$ (n = 0, 1, and 2). *Microporous Mesoporous Mater.*, **153**, 227–235.
100 Zhang, L., van Laak, A.N.C., de Jongh, P.E., and de Jong, K.P. (2009) Synthesis of large mordenite crystals with different aspect ratios. *Microporous Mesoporous Mater.*, **126**, 115–124.
101 Kornatowski, J., Zadrozna, G., Rozwadowski, M., Zibrowius, B., Marlow, F., and Lercher, J.A. (2001) New strategy for chromium substitution and crystal morphology control synthesis and characteristics of CrAPO-5. *Chem. Mater.*, **13**, 4447–4456.
102 Jegatheeswaran, S., Cheng, C.-M., and Cheng, C.-H. (2015) Effects of adding alcohols on ZSM-12 synthesis. *Microporous Mesoporous Mater.*, **201**, 24–34.
103 Shao, C., Li, X., Qiu, S., Xiao, F.-S., and Terasaki, O. (2000) Size-controlled synthesis of silicalite-1 single crystals in the presence of benzene-1,2-diol. *Microporous Mesoporous Mater.*, **39**, 117–123.
104 Yao, J., Yu, L., Zhang, L., and Wang, H. (2011) Influence of glycerol cosolvent on the synthesis of size controllable zeolite A. *Mater. Lett.*, **65**, 2304–2306.
105 Scott, G., Thompson, R.W., Dixon, A.G., and Sacco, A. Jr., (1990) The role of triethanolamine in zeolite crystallization. *Zeolites*, **10**, 44–50.
106 Li, M., Zeng, C., and Zhang, L. (2012) Hydrothermal synthesis of SAPO-5 with novel morphologies from hydrogels containing acetic acid and high concentration of triethylamine under neutral or alkaline conditions. *CrystEngComm*, **14**, 3787–3792.
107 Iwasaki, A., Sano, T., and Kiyozumi, Y. (1998) Effect of additives on the growth behavior of silicalite crystal. *Microporous Mesoporous Mater.*, **25**, 119–126.
108 Ban, T., Mitaku, H., Suzuki, C., Matsuba, J., Ohya, Y., and Takahashi, Y. (2005) Crystallization and crystal morphology of silicalite-1 prepared from silica gel using different amines as a base. *J. Cryst. Growth*, **274**, 594–602.
109 Sun, Y., Song, T., Qiu, S., Pang, W., Shen, J., Jiang, D., and Yue, Y. (1995) Synthesis of mordenite single crystals using two silica sources. *Zeolites*, **15**, 745–753.
110 Greń, W., Parker, S.C., Slater, B., and Lewis, D.W. (2010) Structure of zeolite A (LTA) surfaces and the zeolite A/water interface. *J. Phys. Chem. C*, **114**, 9739–9747.
111 Wulff, G. (1901) Zur Frage der Geschwindigkeit des Wachstums und der Auflösung von Krystallflächen. *Z. Krystallogr. Mineral.*, **34**, 449–530.
112 Lobo, A.J. (2012) Modelling structure direction and morphology control in zeolite synthesis. PhD thesis, University College London. Available at http://discovery.ucl.ac.uk/1350100/
113 Brent, R., Lobo, A.J.W., Lewis, D.W., and Anderson, M.W. (2010) Modifying the crystal habit of zeolite L by addition of an organic space filler. *J. Phys. Chem. C*, **114**, 18240–18246.
114 Guo, P., Shin, J., Greenaway, A.G., Min, J.G., Su, J., Choi, H.J., Liu, L., Cox, P.A., Hong, S.B., Wright, P.A., and Zou, X. (2015) A zeolite family with expanding structural complexity and embedded isoreticular structures. *Nature*, **524**, 74–78.
115 Egerton, R.F. (2012) Mechanisms of radiation damage in beam-sensitive specimens, for TEM accelerating voltages between 10 and 300 kV. *Microsc. Res. Technol.*, **75**, 1550–1556.

116 Csencsits, R. and Gronsky, R. (1987) Damage of zeolite Y in the TEM and its effects on TEM images. *Ultramicroscopy*, **23**, 421–431.

117 Kumar, P., Agrawal, K.V., Tsapatsis, M., and Mkhoyan, K.A. (2015) Quantification of thickness and wrinkling of exfoliated two-dimensional zeolite nanosheets. *Nat. Commun.*, **6**, 7128.

118 Chester, A.W. and Derouane, E.G. (2009) *Zeolite Chemistry and Catalysis*, Springer, Dordrecht, The Netherlands.

119 Speakman, S.A. (2016) Estimating crystallite size using XRD. http://prism.mit.edu/xray/documents/5a%20Estimating%20Crystallite%20Size%20Using%20XRD.pptx (accessed March 2016).

120 Bleken, B.-T.L., Wragg, D.S., Arstad, B., Gunnæs, A.E., Mouzon, J., Helveg, S., Lundegaard, L.F., Beato, P., Bordiga, S., Olsbye, U., Svelle, S., and Lillerud, K.P. (2013) Unit cell thick nanosheets of zeolite H-ZSM-5: structure and activity. *Top. Catal.*, **56**, 558–566.

121 Weisz, P.B. and Frilette, V.J. (1960) Intracrystalline and molecular-shape-selective catalysis by zeolite salts. *J. Phys. Chem.*, **64**, 382.

122 Chang, C.D. (1992) The New Zealand gas-to-gasoline plant: an engineering tour de force. *Catal. Today*, **13**, 103–111.

123 Baerlocher, C., McCusker, L.B., and Olson, D.H. (2007) *Atlas of Zeolite Framework Types*, 6th edn, Elsevier, Amsterdam.

124 Dahl, I.M. and Kolboe, S. (1996) On the reaction mechanism for hydrocarbon formation from methanol over SAPO-34: 2. Isotopic labeling studies of the co-reaction of propene and methanol. *J. Catal.*, **161**, 304–309.

125 Dahl, I.M. and Kolboe, S. (1994) On the reaction mechanism for hydrocarbon formation from methanol over SAPO-34: isotopic labeling studies of the co-reaction of ethene and methanol. *J. Catal.*, **149**, 458–464.

126 Dahl, I.M. and Kolboe, S. (1993) On the reaction mechanism for propene formation in the MTO reaction over SAPO-34. *Catal. Lett.*, **20**, 329–336.

127 Haw, J.F., Song, W., Marcus, D.M., and Nicholas, J.B. (2003) The mechanism of methanol to hydrocarbon catalysis. *Acc. Chem. Res.*, **36**, 317–326.

128 Bjørgen, M., Svelle, S., Joensen, F., Nerlov, J., Kolboe, S., Bonino, F., Palumbo, L., Bordiga, S., and Olsbye, U. (2007) Conversion of methanol to hydrocarbons over zeolite H-ZSM-5: on the origin of the olefinic species. *J. Catal.*, **249**, 195–207.

129 Arstad, B. and Kolboe, S. (2001) The reactivity of molecules trapped within the SAPO-34 cavities in the methanol-to-hydrocarbons reaction. *J. Am. Chem. Soc.*, **123**, 8137–8138.

130 Hereijgers, B.P.C., Bleken, F., Nilsen, M.H., Svelle, S., Lillerud, K.-P., Bjorgen, M., Weckhuysen, B.M., and Olsbye, U. (2009) Product shape selectivity dominates the methanol-to-olefins (MTO) reaction over H-SAPO-34 catalysts. *J. Catal.*, **264**, 77–87.

131 Thiele, E.W. (1939) Relation between catalytic activity and size of particle. *Ind. Eng. Chem. Fund.*, **31**, 916–920.

132 Tosheva, L. and Valtchev, V.P. (2005) Nanozeolites: synthesis, crystallization mechanism, and applications. *Chem. Mater.*, **17**, 2494–2513.

133 Wu, L., Magusin, P.C.M.M., Degirmenci, V., Li, M., Almutairi, S.M.T., Zhu, X., Mezari, B., and Hensen, E.J.M. (2014) Acidic properties of nanolayered ZSM-5 zeolites. *Microporous Mesoporous Mater.*, **189**, 144–157.

134 Lee, Y.-J., Baek, S.-C., and Jun, K.-W. (2007) Methanol conversion on SAPO-34 catalysts prepared by mixed template method. *Appl. Catal., A*, **329**, 130–136.

135 Yang, G., Wei, Y., Xu, S., Chen, J., Li, J., Liu, Z., Yu, J., and Xu, R. (2013) Nanosize-enhanced lifetime of SAPO-34 catalysts in methanol-to-olefin reactions. *J. Phys. Chem. C*, **117**, 8214–8222.

136 Li, Z., Martinez-Triguero, J., Concepcion, P., Yu, J., and Corma, A. (2013) Methanol to olefins: activity and stability of nanosized SAPO-34 molecular sieves and control of selectivity by silicon distribution. *Phys. Chem. Chem. Phys.*, **15**, 14670–14680.

137 Alvaro-Munoz, T., Sastre, E., and Marquez-Alvarez, C. (2014) Microwave-assisted synthesis of plate-like SAPO-34 nanocrystals with increased catalyst lifetime in the methanol-to-olefin reaction. *Catal. Sci. Technol.*, **4**, 4330–4339.

138 Barger, P. (2011) Methanol to olefins (MTO) and beyond, in *Zeolites for Cleaner Technologies*, Imperial College Press, pp. 239–260.

139 Dai, W., Wu, G., Li, L., Guan, N., and Hunger, M. (2013) Mechanisms of the deactivation of SAPO-34 materials with different crystal sizes applied as MTO catalysts. *ACS Catal.*, **3**, 588–596.

140 Lee, K.Y., Chae, H.-J., Jeong, S.-Y., and Seo, G. (2009) Effect of crystallite size of SAPO-34 catalysts on their induction period and deactivation in methanol-to-olefin reactions. *Appl. Catal. A*, **369**, 60–66.

141 Nishiyama, N., Kawaguchi, M., Hirota, Y., Van Vu, D., Egashira, Y., and Ueyama, K. (2009) Size control of SAPO-34 crystals and their catalyst lifetime in the methanol-to-olefin reaction. *Appl. Catal. A*, **362**, 193–199.

142 Ye, L., Cao, F., Ying, W., Fang, D., and Sun, Q. (2011) Effect of different TEAOH/DEA combinations on SAPO-34's synthesis and catalytic performance. *J. Porous Mater.*, **18**, 225–232.

143 Sugimoto, M., Katsuno, H., Takatsu, K., and Kawata, N. (1987) Correlation between the crystal size and catalytic properties of ZSM-5 zeolites. *Zeolites*, **7**, 503–507.

144 Losch, P., Boltz, M., Louis, B., Chavan, S., and Olsbye, U. (2015) Catalyst optimization for enhanced propylene formation in the methanol-to-olefins reaction. *C. R. Chim.*, **18**, 330–335.

145 Bleken, F.L., Chavan, S., Olsbye, U., Boltz, M., Ocampo, F., and Louis, B. (2012) Conversion of methanol into light olefins over ZSM-5 zeolite: strategy to enhance propene selectivity. *Appl. Catal. A*, **447–448**, 178–185.

146 Hartmann, M. (2004) Hierarchical zeolites: a proven strategy to combine shape selectivity with efficient mass transport. *Angew. Chem., Int. Ed.*, **43**, 5880–5882.

147 Schmidt, F., Paasch, S., Brunner, E., and Kaskel, S. (2012) Carbon templated SAPO-34 with improved adsorption kinetics and catalytic performance in the MTO-reaction. *Microporous Mesoporous Mater.*, **164**, 214–221.

148 Yang, H., Liu, Z., Gao, H., and Xie, Z. (2010) Synthesis and catalytic performances of hierarchical SAPO-34 monolith. *J. Mater. Chem.*, **20**, 3227–3231.

149 Yang, S.-T., Kim, J.-Y., Chae, H.-J., Kim, M., Jeong, S.-Y., and Ahn, W.-S. (2012) Microwave synthesis of mesoporous SAPO-34 with a hierarchical pore structure. *Mater. Res. Bull.*, **47**, 3888–3892.

150 Alvaro-Munoz, T., Marquez-Alvarez, C., and Sastre, E. (2013) Effect of silicon content on the catalytic behavior of chabazite type silicoaluminophosphate in the transformation of methanol to short chain olefins. *Catal. Today*, **213**, 219–225.

151 Na, K., Chol, M., Park, W., Sakamoto, Y., Terasakl, O., and Ryoo, R. (2010) Pillared MFI zeolite nanosheets of a single-unit-cell thickness. *J. Am. Chem. Soc.*, **132**, 4169–4177.

152 Svelle, S., Joensen, F., Nerlov, J., Olsbye, U., Lillerud, K.P., Kolboe, S., and Bjørgen, M. (2006) Conversion of methanol into hydrocarbons over zeolite H-ZSM-5: ethene formation is mechanistically separated from the formation of higher alkenes. *J. Am. Chem. Soc.*, **128**, 14770–14771.

153 Khare, R., Millar, D., and Bhan, A. (2015) A mechanistic basis for the effects of crystallite size on light olefin selectivity in methanol-to-hydrocarbons conversion on MFI. *J. Catal.*, **321**, 23–31.

154 Ilias, S., Khare, R., Malek, A., and Bhan, A. (2013) A descriptor for the relative propagation of the aromatic- and olefin-based cycles in methanol-to-hydrocarbons conversion on H-ZSM-5. *J. Catal.*, **303**, 135–140.

155 Teketel, S., Svelle, S., and Beato, P. (2013) Catalyst for the conversion of oxygenates to olefins and a process for preparing said

catalyst. Patent No. WO 2013014081; US Patent 2014/0179971.

156 Teketel, S., Lundegaard, L.F., Skistad, W., Chavan, S.M., Olsbye, U., Lillerud, K.P., Beato, P., and Svelle, S. (2015) Morphology-induced shape selectivity in zeolite catalysis. *J. Catal.*, **327**, 22–32.

157 Teketel, S., Skistad, W., Benard, S., Olsbye, U., Lillerud, K.P., Beato, P., and Svelle, S. (2012) Shape selectivity in the conversion of methanol to hydrocarbons: the catalytic performance of one-dimensional 10-ring zeolites: ZSM-22, ZSM-23, ZSM-48, and EU-1. *ACS Catal.*, **2**, 26–37.

158 Bleken, F., Skistad, W., Barbera, K., Kustova, M., Bordiga, S., Beato, P., Lillerud, K.P., Svelle, S., and Olsbye, U. (2011) Conversion of methanol over 10-ring zeolites with differing volumes at channel intersections: comparison of TNU-9, IM-5, ZSM-11 and ZSM-5. *Phys. Chem. Chem. Phys.*, **13**, 2539–2549.